Dark matter-electron interactions in materials beyond the dark photon model

N.B. When citing this work, cite the original published paper.

(article starts on next page)

PAPER • OPEN ACCESS

Dark matter-electron interactions in materials beyond the dark photon model

To cite this article: Riccardo Catena *et al* JCAP03(2023)052

View the article online for updates and enhancements.

Dark matter-electron interactions in materials beyond the dark photon model

Riccardo Catena,[a] **Daniel Cole,**[a] **Timon Emken,**[b] **Marek Matas,**[c] **Nicola Spaldin,**[c] **Walter Tarantino**[c] **and Einar Urdshals**[a]

[a]Department of Physics, Chalmers University of Technology,
SE-412 96 Göteborg, Sweden

[b]The Oskar Klein Centre, Department of Physics, Stockholm University,
AlbaNova, SE-10691 Stockholm, Sweden

[c]Department of Materials, ETH Zürich,
CH-8093 Zürich, Switzerland

E-mail: catena@chalmers.se, guscoleda@student.gu.se, timon.emken@fysik.su.se, marek.matas@mat.ethz.ch, nicola.spaldin@mat.ethz.ch, wtarantino@dsf.unica.it, urdshals@chalmers.se

Abstract. The search for sub-GeV dark matter (DM) particles via electronic transitions in underground detectors attracted much theoretical and experimental interest in the past few years. A still open question in this field is whether experimental results can in general be interpreted in a framework where the response of detector materials to an external DM probe is described by a single ionisation or crystal form factor, as expected for the so-called dark photon model. Here, ionisation and crystal form factors are examples of material response functions: interaction-specific integrals of the initial and final state electron wave functions. In this work, we address this question through a systematic classification of the material response functions induced by a wide range of models for spin-0, spin-1/2 and spin-1 DM. We find several examples for which an accurate description of the electronic transition rate at DM direct detection experiments requires material response functions that go beyond those expected for the dark photon model. This concretely illustrates the limitations of a framework that is entirely based on the standard ionisation and crystal form factors, and points towards the need for the general response-function-based formalism we pushed forward recently [1, 2]. For the models that require non-standard atomic and crystal response functions, we use the response functions of [1, 2] to calculate the DM-induced electronic transition rate in atomic and crystal detectors, and to present 90% confidence level exclusion limits on the strength of the DM-electron interaction from the null results reported by XENON10, XENON1T, EDELWEISS and SENSEI.

Contents

1 Introduction

The nature of the dark matter (DM) component of the universe, whose gravitational effects are visible from local to cosmological scales, remains elusive. The leading hypothesis in astroparticle physics is that DM is made of new, yet undetected particles [3]. Direct detection experiments play a crucial role in the quest for the DM particle, and search for DM scattering events in low-background detectors located deep underground [4–6]. So far, this class of experiments has focused on the search for the Weakly Interacting Massive Particle (WIMP): a DM candidate of mass between few GeV and tens of TeV that interacts with the known particles with weak scale interactions, and predicted by theories which were not initially formulated in a DM context, e.g. supersymmetry [7, 8]. The lack of an unambiguous WIMP

detection has recently motivated a systematic, theoretical and experimental exploration of alternative paradigms [9].

An alternative scenario that could explain why WIMPs have so far escaped detection is the one where DM is lighter than the nucleons bound to nuclei, and thus too light to induce an observable nuclear recoil in a direct detection experiment [10]. An interesting aspect of this scenario is that it is testable, as a Milky Way DM particle in the keV-GeV mass range would have enough kinetic energy to cause an observable electronic transition in a detector material, provided it interacts strongly enough with the constituent electrons [11]. Being a testable explanation for the lack of WIMP discovery, the sub-GeV DM paradigm has recently attracted much attention [9, 12]. In particular, a variety of experimental tests has been proposed or performed to probe this idea. This includes the search for: atomic ionisations in noble gas xenon and argon detectors [1, 11, 13–16], electronic transitions in semiconductor crystals [2, 17–30] as well as in superconductors [31, 32] and 3D Dirac materials [33–35], electron ejections from graphene [36] and carbon nanotubes [37], and collective phenomena such as phonons [38, 39] and magnons [40]. This is an incomplete list, and we refer to [9, 12] for an extended review of the field.

A central element in the development and implementation of the experimental tests mentioned above is the theoretical modelling of DM-electron interactions. Typically, the interactions between DM particles and electrons are described within the "dark photon model", which extends the Standard Model of particle physics by an additional U(1) gauge group under which only the DM particle is charged [10, 41–44]. In this model, the DM-electron interaction arises from the "kinetic mixing" between the ordinary photon and the gauge boson associated with the new U(1) group, i.e. the dark photon. A crucial prediction of the model is that the response of materials to DM-electron interactions depends on a single, material-specific ionisation or crystal form factor [18]. While the dark photon model has extensively been used in the interpretation of results from DM direct detection experiments, it is also a rather restrictive framework, as it a priori neglects DM-electron couplings that are allowed by observations, and assumes that the interactions between DM and electrons are necessarily mediated by a spin-1 particle. Furthermore, the model is often complemented by the additional assumption that the DM particle has either spin 0 or 1/2. However, there is no experimental evidence supporting these restrictions and, therefore, a more general approach is in many respects preferable.

In order to develop a description of DM-electron scattering in detector materials that goes beyond the one of the dark photon model, we recently developed a non-relativistic effective theory for the scattering of Milky Way DM particles by the electrons bound to isolated atoms [1] or semiconductor crystals [2]. This allowed us to systematically classify the interactions between DM particles and electrons in terms of a finite set of Galilean and rotational invariant quantum mechanical operators that are defined in the DM-electron spin space. Virtually any DM particle theory can be mapped onto a linear combination of such operators with momentum transfer dependent coefficients. Importantly, this general approach to the theoretical modelling of DM-electron interactions predicts that up to four (for isolated atoms) and up to five (for crystals) electron wave function overlap integrals, or "response functions", are required in order to accurately describe the scattering of DM particles by the electrons bound in detector materials. In other words, the response of materials to an external DM perturbation can in principle be significantly different from the one predicted by the dark photon model. Recently, our formalism was adopted by the XENON collaboration to analyse their latest S2-only data from XENON1T [45].

A still open question in this field is whether the novel material response functions we identified in [1] and [2] are indeed important in the interpretation of DM direct detection experiments, or they only appear in marginal models. While in [1, 2] we provided relevant examples, such as the anapole or magnetic dipole DM models, where our "response function" formalism is crucial to accurately predict observable electronic transition rates, a systematic classification of the DM-electron interaction models that can generate a non-standard material response to an external DM perturbation is still missing. Answering this question is important, as it would clarify whether present and future DM direct detection experiments can indeed be interpreted within a framework that entirely relies on a single ionisation or crystal form factor, or a general analysis of the response to DM-electron interactions of detector materials is crucial.

In this work, we answer the above question by calculating the rate of electronic transitions induced by the non-relativistic scattering of DM particles by electrons bounds to isolated atoms or silicon and germanium crystals for a wide range of models for spin-0, spin-1/2 and spin-1 DM. Remarkably, we find eight relativistic Lagrangians which in the non-relativistic limit predict a non-standard material response to external DM-electron interactions. This corroborates the results we reported in [1, 2] and shows the importance of a "response function" formalism in the interpretation of DM direct detection experiments. This work is organised as follows. In section 2, we introduce the relativistic models for DM-electron interactions we are interested in. In section 3 we calculate the rate of DM-induced electronic transitions in atoms or crystals predicted by the models of section 2 within the response function formalism of [1, 2]. Here, we also show that the response functions for xenon, germanium and silicon can be expressed within a unified formalism that allows for a direct comparison of different target materials. Finally, in section 4, we compare our theoretical predictions with the null results reported by the XENON10 [46], XENON1T [15], EDELWEISS [23] and SENSEI [24] DM direct detection experiments, setting 90% confidence level upper bounds on the coupling constants of the models we consider in this work. We summarise and conclude in section 5, and refer to three appendices for the details of our calculations, useful identities and complementary results.

2 General models for dark matter-electron interactions

This section introduces the framework we use to describe DM-electron interactions in detector materials.

In the interpretation of data from direct detection experiments, DM-electron interactions are typically described within the so-called dark photon model [42] (for a review, see also [10] and references therein). This framework extends the Standard Model of particle physics by an additional U(1) gauge group and by a DM candidate. Only the DM particle is charged under the new gauge group, while a "kinetic mixing" between ordinary and dark photon generates the interactions between the electrically charged particles in the Standard Model and the DM candidate, which, within this framework, typically consists of either scalar or fermionic particles. Here, by "dark photon" one refers to the gauge boson associated with the new U(1) group.

In this work, we extend the standard dark photon model in three ways. First, we consider both spin-0 and spin-1 particles as "mediators" of the DM-electron interaction, without restricting ourselves to vector mediators, as in the dark photon model. Second, we focus on DM-mediator interaction vertices with a general Lorentz structure. In contrast, in the dark photon model only interactions arising from a kinetic mixing are considered. Finally, we allow for DM to have spin 0, spin 1/2 or spin 1. These extensions are motivated by the

lack of an experimentally preferred model for sub-GeV DM, which, in our view, should be compensated by a general approach to the theoretical modelling of DM-electron interactions. The main implication of these extensions is that in the models we consider here the response of detector materials to DM-electron interactions cannot be described via the canonical "form factors" introduced within the dark photon model. As we will see below, it must be modelled within the "response function" formalism we developed by using effective theory methods in [1], for isolated atoms, and in [2], for crystals. From this point of view, the analysis presented here provide a crucial, concrete application of the formalism we established in [1, 2], which is therefore proven to be relevant and important in the theoretical modelling of DM-electron interactions. Furthermore, it also shows how the effective operators identified in [1, 2] can arise from the non-relativistic reduction of relativistic theories for DM-electron interactions. Below, we introduce the models we are interested in, focusing on scalar, fermionic and vector DM separately.

Notice that the models we consider here do not provide a mechanism for the DM particle and mediator mass generation, and should therefore be completed in the high-energy (i.e. ultra-violet) limit. While this completion is expected to introduce new, phenomenologically interesting particles, it goes beyond the purposes of this work. Therefore, we refer to [7] and references therein for a review of possible ultra-violet completions of the models introduced below.

2.1 Scalar dark matter

Let us start by introducing our models for spin-0 DM. Here, we denote by S the complex scalar that describes the DM particle, and consider two cases for the particle that mediates the DM-electron interactions, i.e. "the mediator". In the first case, we assume a spin-0 particle of mass m_ϕ described by the real scalar field ϕ. In the second case we assume a spin-1 particle of mass m_G described by the real vector G_μ. In the case of a scalar mediator, ϕ, we introduce the Lagrangian

$$
\begin{aligned}
\mathcal{L}_{S\phi e} = {} & \partial_\mu S^\dagger \partial^\mu S - m_S^2 S^\dagger S - \frac{\lambda_S}{2}(S^\dagger S)^2 \\
& + \frac{1}{2}\partial_\mu \phi \partial^\mu \phi - \frac{1}{2}m_\phi^2 \phi^2 - \frac{m_\phi \mu_1}{3}\phi^3 - \frac{\mu_2}{4}\phi^4 \\
& + i\bar{e}\slashed{D}e - m_e \bar{e}e \\
& - g_1 m_S S^\dagger S \phi - \frac{g_2}{2} S^\dagger S \phi^2 - h_1 \bar{e}e\phi - ih_2 \bar{e}\gamma^5 e\phi \,,
\end{aligned}
\tag{2.1}
$$

where m_S is the DM mass, while λ_S, μ_1, μ_2, g_1, g_2, h_1, and h_2 are coupling constants. In eq. (2.1), m_e and e are the electron mass and Dirac spinor, respectively. On the other hand, when the interaction between DM particles and electrons is mediated by a spin-1 particle, we assume

$$
\begin{aligned}
\mathcal{L}_{SGe} = {} & \partial_\mu S^\dagger \partial^\mu S - m_S^2 S^\dagger S - \frac{\lambda_S}{2}(S^\dagger S)^2 \\
& - \frac{1}{4}\mathcal{G}_{\mu\nu}\mathcal{G}^{\mu\nu} + \frac{1}{2}m_G^2 G_\mu G^\mu - \frac{\lambda_G}{4}(G_\mu G^\mu)^2 \\
& + i\bar{e}\slashed{D}e - m_e \bar{e}e \\
& - \frac{g_3}{2} S^\dagger S G_\mu G^\mu - ig_4(S^\dagger \partial_\mu S - \partial_\mu S^\dagger S)G^\mu \\
& - h_3(\bar{e}\gamma_\mu e)G^\mu - h_4(\bar{e}\gamma_\mu \gamma^5 e)G^\mu \,,
\end{aligned}
\tag{2.2}
$$

where λ_G, g_1, g_2, h_1, and h_2 are coupling constants, while $\mathcal{G}_{\mu\nu}$ is the field strength tensor for G_μ.

2.2 Fermionic dark matter

We now focus on the case of spin-1/2 DM with mass m_χ. When the interactions between the DM particles and electrons are mediated by a scalar particle of mass m_ϕ, we assume the Lagrangian,

$$
\begin{aligned}
\mathcal{L}_{\chi\phi e} = {}& i\overline{\chi}\slashed{\partial}\chi - m_\chi\overline{\chi}\chi \\
& + \frac{1}{2}\partial_\mu\phi\partial^\mu\phi - \frac{1}{2}m_\phi^2\phi^2 - \frac{m_\phi\mu_1}{3}\phi^3 - \frac{\mu_2}{4}\phi^4 \\
& + i\overline{e}\slashed{\partial}e - m_e\overline{e}e \\
& - \lambda_1\phi\overline{\chi}\chi - i\lambda_2\phi\overline{\chi}\gamma^5\chi - h_1\phi\overline{e}e - ih_2\phi\overline{e}\gamma^5 e \,,
\end{aligned}
\tag{2.3}
$$

where λ_1 and λ_2 are coupling constants, while χ is the Dirac spinor that describes the DM particle. Alternatively, in the case of a vector mediator, G_μ, we assume the following Lagrangian

$$
\begin{aligned}
\mathcal{L}_{\chi G e} = {}& i\overline{\chi}\slashed{\partial}\chi - m_\chi\overline{\chi}\chi \\
& - \frac{1}{4}\mathcal{G}_{\mu\nu}\mathcal{G}^{\mu\nu} + \frac{1}{2}m_G^2 G_\mu G^\mu - \frac{\lambda_G}{4}(G_\mu G^\mu)^2 \\
& + i\overline{e}\slashed{\partial}e - m_e\overline{e}e \\
& - \lambda_3\overline{\chi}\gamma^\mu\chi G_\mu - \lambda_4\overline{\chi}\gamma^\mu\gamma^5\chi G_\mu \\
& - h_3\overline{e}\gamma_\mu e G^\mu - h_4\overline{e}\gamma_\mu\gamma^5 e G^\mu \,,
\end{aligned}
\tag{2.4}
$$

where h_3 and h_4 are additional coupling constants, and the remaining symbols were introduced above.

2.3 Vector dark matter

Finally, we focus on the case of spin-1 DM particles with mass m_X described by a complex vector field, X_μ. For DM-electron interactions mediated by a scalar field, ϕ, we assume the Lagrangian,

$$
\begin{aligned}
\mathcal{L}_{X\phi e} = {}& -\frac{1}{2}\mathcal{X}_{\mu\nu}^\dagger\mathcal{X}^{\mu\nu} + m_X^2 X_\mu^\dagger X^\mu - \frac{\lambda_X}{2}(X_\mu^\dagger X^\mu)^2 \\
& + \frac{1}{2}(\partial_\mu\phi)^2 - \frac{1}{2}m_\phi^2\phi^2 - \frac{m_\phi\mu_1}{3}\phi^3 - \frac{\mu_2}{4}\phi^4 \\
& + i\overline{e}\slashed{\partial}e - m_e\overline{e}e \\
& - b_1 m_X \phi X_\mu^\dagger X^\mu - \frac{b_2}{2}\phi^2 X_\mu^\dagger X^\mu \\
& - h_1\phi\overline{e}e - ih_2\phi\overline{e}\gamma^5 e \,,
\end{aligned}
\tag{2.5}
$$

where λ_X, b_1 and b_2 are new coupling constants, and $\mathcal{X}_{\mu\nu}$ is the field strength tensor for X_μ. On the other hand, in the case of DM-electron interactions mediated by a spin-1 particle,

we assume

$$\mathcal{L}_{XGe} = -\frac{1}{2}\mathcal{X}^\dagger_{\mu\nu}\mathcal{X}^{\mu\nu} + m_X^2 X_\mu^\dagger X^\mu - \frac{\lambda_X}{2}(X_\mu^\dagger X^\mu)^2$$
$$- \frac{1}{4}\mathcal{G}_{\mu\nu}\mathcal{G}^{\mu\nu} + \frac{1}{2}m_G^2 G_\mu G^\mu - \frac{\lambda_G}{4}(G_\mu G^\mu)^2$$
$$+ i\bar{e}\slashed{D}e - m_e\bar{e}e$$
$$- \frac{b_3}{2}G_\mu G^\mu(X_\nu^\dagger X^\nu) - \frac{b_4}{2}(G^\mu G^\nu)(X_\mu^\dagger X_\nu)$$
$$- \Big[ib_5 X_\nu^\dagger \partial_\mu X^\nu G^\mu + b_6 X_\mu^\dagger \partial^\mu X_\nu G^\nu$$
$$+ b_7 \varepsilon_{\mu\nu\rho\sigma}(X^{\dagger\mu}\partial^\nu X^\rho)G^\sigma + \text{h.c.}\Big]$$
$$- h_3 G_\mu \bar{e}\gamma^\mu e - h_4 G_\mu \bar{e}\gamma^\mu\gamma^5 e\,, \tag{2.6}$$

where b_3, b_4, b_5, b_6 and b_7 are coupling constants. Contrary to all other coupling constants, which can without loss of generality be assumed to be real, b_6 and b_7 are in general complex variables [47].

3 Expected rate of electron transitions in detector materials

From the Lagrangians introduced in section 2, we now calculate the expected rate of electron transitions induced by DM scattering in isolated atoms and crystals. We start by reviewing the results of [1, 2] (section 3.1). We then apply these results to the general models of section 2 (section 3.2).

3.1 General considerations

Let us consider the scattering of a DM particle of mass $m_{\rm DM}$, initial velocity in the detector rest frame $\boldsymbol{v}$, and momentum $\boldsymbol{p} = m_{\rm DM}\boldsymbol{v}$ by an electron bound to an isolated atom or to a crystal, and described by the initial state $|\mathbf{e}_1\rangle$. Furthermore, let us denote by $|\mathbf{e}_2\rangle$ the state of the outgoing electron, and by $\boldsymbol{p}'$ the momentum of the final state DM particle. The momentum transfer in the scattering is thus $\boldsymbol{q} = \boldsymbol{p} - \boldsymbol{p}'$, and the rate for the $|\mathbf{e}_1\rangle$ to $|\mathbf{e}_2\rangle$ transition is given by [1, 2]

$$\mathscr{R}_{1\to 2} = \frac{n_{\rm DM}}{16 m_{\rm DM}^2 m_e^2} \int \frac{\mathrm{d}^3 q}{(2\pi)^3} \int \mathrm{d}^3 \boldsymbol{v}\, f(\boldsymbol{v})(2\pi)\delta(E_f - E_i)\overline{|\mathcal{M}_{1\to 2}|^2}\,, \tag{3.1}$$

where E_i and E_f are the total initial and final energy, respectively. They can be written as follows

$$E_i = m_{\rm DM} + m_e + \frac{|\boldsymbol{p}|^2}{2m_{\rm DM}} + E_1$$
$$E_f = m_{\rm DM} + m_e + \frac{|\boldsymbol{p} - \boldsymbol{q}|^2}{2m_{\rm DM}} + E_2\,. \tag{3.2}$$

Here, $E_1 < 0$ ($E_2 > 0$) is the energy eigenvalue of the state $|\mathbf{e}_1\rangle$ ($|\mathbf{e}_2\rangle$). This convention for the signs of E_1 and E_2 reflects our interest in transitions from bound atomic (valence) to free (conduction) states (see sections 3.1.1 and 3.1.2). In eq. (3.1), $\mathcal{M}_{1\to 2}$ is the electron transition amplitude, defined as the overlap integral,

$$\mathcal{M}_{1\to 2}(\boldsymbol{q}, \boldsymbol{v}) = \int \frac{\mathrm{d}^3 \boldsymbol{\ell}}{(2\pi)^3} \widetilde{\psi}_2^*(\boldsymbol{\ell} + \boldsymbol{q})\, \mathcal{M}(\boldsymbol{q}, \boldsymbol{v}_{\rm el}^\perp(\boldsymbol{v}, \boldsymbol{q}, \boldsymbol{\ell}))\, \widetilde{\psi}_1(\boldsymbol{\ell})\,, \tag{3.3}$$

where $\widetilde{\psi}_1$ ($\widetilde{\psi}_2$) is the Fourier transform of ψ_1 (ψ_2), while ψ_1 (ψ_2) is the wave function associated with the state $|\mathbf{e}_1\rangle$ ($|\mathbf{e}_2\rangle$), and $\mathcal{M}$ is the free electron scattering amplitude. In the *non-relativistic*, elastic scattering of a DM particle by free electrons, $\mathcal{M}$ uniquely depends on the momentum transfer $\boldsymbol{q}$ and on the transverse relative velocity $\boldsymbol{v}_{\rm el}^\perp = \boldsymbol{v} - \boldsymbol{q}/(2\mu_{\rm DMe}) - \boldsymbol{\ell}/m_e$, where $\mu_{\rm DMe}$ is the DM-electron reduced mass and $\boldsymbol{\ell}$ is the initial state electron momentum. This simplification is a consequence of Galilean invariance (that is, the invariance under constant shifts of particle velocities) and three-dimensional momentum conservation, which allow one to express $\mathcal{M}$ as a function of two kinematic variables only (see [1, 2, 48–50] for further details). Notice that Galilean invariance is fulfilled when both the DM particle and the electron are non-relativistic. We can now expand $\mathcal{M}$ at linear order in $\boldsymbol{\ell}/m_e$, which implies [1, 2],

$$\mathcal{M}_{1\to2}(\boldsymbol{q},\boldsymbol{v}) \simeq \mathcal{M}(\boldsymbol{q},\boldsymbol{v}_{\rm el}^\perp)\big|_{\boldsymbol{\ell}=\mathbf{0}}\, f_{1\to2}(\boldsymbol{q}) + m_e\,\nabla_{\boldsymbol{\ell}}\mathcal{M}(\boldsymbol{q},\boldsymbol{v}_{\rm el}^\perp)\big|_{\boldsymbol{\ell}=\mathbf{0}}\cdot\boldsymbol{f}_{1\to2}(\boldsymbol{q})\,, \qquad (3.4)$$

where in the right-hand-side we introduced the scalar and vectorial wave function overlap integrals,

$$f_{1\to2}(\boldsymbol{q}) \equiv \int \mathrm{d}^3\mathbf{x}\,\psi_2^*(\mathbf{x})\,e^{i\boldsymbol{q}\cdot\mathbf{x}}\,\psi_1(\mathbf{x})\,, \qquad (3.5)$$

$$\boldsymbol{f}_{1\to2}(\boldsymbol{q}) \equiv \int \mathrm{d}^3\mathbf{x}\,\psi_2^*(\mathbf{x})\,e^{i\boldsymbol{q}\cdot\mathbf{x}}\,\frac{i\nabla_{\mathbf{x}}}{m_e}\psi_1(\mathbf{x})\,. \qquad (3.6)$$

In eq. (3.1), $n_{\rm DM} = \rho_{\rm DM}/m_{\rm DM}$ is the local DM number density, $\rho_{\rm DM} = 0.4\,\mathrm{GeV\,cm^{-3}}$ the local DM mass density [51], and $f(\boldsymbol{v})$ the local DM velocity distribution boosted to the detector rest frame. For $f(\boldsymbol{v})$, we assume a truncated Maxwell-Boltzmann distribution with local standard of rest speed $v_0 = 238\,\mathrm{km\,s^{-1}}$ [52], galactic escape speed $v_{\rm esc} = 544\,\mathrm{km\,s^{-1}}$ [52] and Earth's speed in the galactic frame (where the mean DM particle velocity is zero) $v_e = 250.5\,\mathrm{km\,s^{-1}}$ [52].

The *theoretical* rate of DM-induced electron transitions in a detector material, $\mathscr{R}_{\rm theory}$, is related to the rate for state $|\mathbf{e}_1\rangle$ to state $|\mathbf{e}_2\rangle$ transitions, $\mathscr{R}_{1\to2}$, by a sum over all "relevant" initial and final states. For detectors that can be approximated by a system of isolated atoms, and that search for atomic ionisations induced by the scattering of DM particles in the detector, the relevant initial states are bound states characterised by the principal, angular and magnetic quantum numbers, n, ℓ and m, respectively. The relevant final states are free electron states characterised by an "asymptotic" momentum k', and by the electron angular and magnetic quantum numbers, ℓ' and m', respectively. We refer to the appendices of [1] for an explicit form of the corresponding wave functions. By replacing 1 with the quantum numbers $\{n\ell m\}$, and 2 with $\{k'\ell'm'\}$ in eq. (3.4), and inserting eq. (3.4) into eq. (3.1), we obtain

$$\mathscr{R}_{\rm theory} = \mathscr{R}_{\rm ion} \equiv 2\sum_{n,\ell}\sum_{m=-\ell}^{\ell}\sum_{\ell'=0}^{\infty}\sum_{m'=-\ell'}^{\ell'}\int \mathrm{d}k'\,\frac{Vk'^2}{(2\pi)^3}\mathscr{R}_{n\ell m\to k'\ell'm'}\,, \qquad (3.7)$$

where the (ℓ,m) sum runs over the outermost occupied orbitals, e.g. the 4s, 4p, 4d, 5s, and 5p orbitals in the case of xenon atoms, which is of interest for the present work. In eq. (3.7) we assume that wave functions have been normalised over a finite volume V, and the overall factor of 2 accounts for the double occupation of each electronic state due to spin degeneracy. For crystal detectors that search for electronic transitions from valence to conduction bands

in semiconductor targets, the relevant initial states are occupied valence states labeled by a band index i and a reciprocal lattice momentum in the first Brillouin Zone (BZ), $\boldsymbol{k}$. Similarly, the relevant final states are in this case unoccupied conduction states characterised by a band index i' and a reciprocal lattice momentum in the first BZ, $\boldsymbol{k}'$. For crystal detectors, we thus find

$$\mathscr{R}_{\text{theory}} = \mathscr{R}_{\text{crystal}} \equiv 2 \sum_{ii'} \int_{\text{BZ}} \frac{V \mathrm{d}^3 k}{(2\pi)^3} \int_{\text{BZ}} \frac{V \mathrm{d}^3 k'}{(2\pi)^3} \, \mathscr{R}_{i\boldsymbol{k} \to i'\boldsymbol{k}'} \, . \tag{3.8}$$

We refer to [2] for an explicit form of the Bloch wave functions $\psi_{i\boldsymbol{k}}$ and $\psi_{i'\boldsymbol{k}'}$ entering eqs. (3.5) and (3.6).

In general, we express the rate $\mathscr{R}_{\text{theory}}$ within our "response function" formalism [1, 2], where

$$\mathscr{R}_{\text{theory}} = \frac{n_{\text{DM}}}{128\pi m_{\text{DM}}^2 m_e^2} \int \mathrm{d}(\ln \Delta E) \int \mathrm{d}q \, q \, \widehat{\eta}\,(q, \Delta E) \sum_{l=1}^{r} \text{Re}\left[\mathcal{R}_l^*(q, v) \overline{\mathcal{W}}_l(q, \Delta E)\right] \, . \tag{3.9}$$

With an appropriate choice of "material response" functions $\overline{\mathcal{W}}_l(q, \Delta E)$, and "DM response" functions $\mathcal{R}_l(q, v)$, eq. (3.9) applies to any detector material and particle physics model. In particular, it applies to detectors that can be approximated by a set of isolated atoms, such as XENON10 and XENON1T, and to crystal detectors, such as SENSEI and EDELWEISS. The velocity operator in eq. (3.9), $\widehat{\eta}\,(q, \Delta E)$, depends on the momentum transfer, $\boldsymbol{q}$, and on the deposited energy, ΔE. It linearly acts on the generic function of velocities, $g(\boldsymbol{v})$, as shown below

$$\widehat{\eta}\,(q, \Delta E)\,[g(\boldsymbol{v})] = \int_{|\boldsymbol{v}| \geq v_{\min}} \mathrm{d}^3 v \, g(\boldsymbol{v}) \frac{f_\chi(\boldsymbol{v})}{v} \, , \tag{3.10}$$

where

$$v_{\min} = \frac{q}{2m_{\text{DM}}} + \frac{\Delta E}{q} \, , \tag{3.11}$$

is the minimum velocity required to transfer a momentum $\boldsymbol{q}$ when the deposited energy is ΔE, and $q \equiv |\boldsymbol{q}|$. Below, we first provide explicit expressions for the $\overline{\mathcal{W}}_l(q, \Delta E)$, $l = 1, \dots r$ functions that characterise detectors consisting of isolated atoms (section 3.1.1) and crystals (section 3.1.2). We then calculate the functions $\mathcal{R}_l(q, v)$, $l = 1, \dots r$, for all models in section 2 (section 3.2).

3.1.1 Isolated atoms

The material response functions $\overline{\mathcal{W}}_l$ are defined via an integral over the azimuthal and polar angles of $\boldsymbol{q}$,

$$\overline{\mathcal{W}}_l(q, \Delta E) \equiv \int \mathrm{d}\Omega_q \, \mathcal{W}_l(\boldsymbol{q}, \Delta E) \, , \tag{3.12}$$

where, for detectors that can be modelled as a sample of isolated atoms, such as XENON10 or XENON1T,

$$\mathcal{W}_l(\boldsymbol{q}, \Delta E) = \frac{2}{\pi} \Delta E \sum_{n,\ell,m} \sum_{\ell',m'} \int \frac{V k'^2 \, \mathrm{d}k'}{(2\pi)^3} \, \mathscr{B}_l \, \delta(\Delta E - E_{k'\ell'm'} + E_{n\ell m}) \, , \tag{3.13}$$

– 8 –

and

$$\mathscr{B}_1 = |f_{n\ell m \to k'\ell'm'}|^2 \tag{3.14}$$

$$\mathscr{B}_2 = \frac{\boldsymbol{q}}{m_e} \cdot (f_{n\ell m \to k'\ell'm'})(\boldsymbol{f}_{n\ell m \to k'\ell'm'})^* \tag{3.15}$$

$$\mathscr{B}_3 = |\boldsymbol{f}_{n\ell m \to k'\ell'm'}|^2 \tag{3.16}$$

$$\mathscr{B}_4 = \left| \frac{\boldsymbol{q}}{m_e} \cdot \boldsymbol{f}_{n\ell m \to k'\ell'm'} \right|^2 . \tag{3.17}$$

$E_{n\ell m}$ ($E_{k'\ell'm'}$) is the energy of the initial (final) state electron and $f_{n\ell m \to k'\ell'm'}$ ($\boldsymbol{f}_{n\ell m \to k'\ell'm'}$) replaces $f_{1\to2}$ ($\boldsymbol{f}_{1\to2}$). To compare the results reported here with those in [1], we note that the $W_l^{n\ell}(k', q)$ functions introduced in [1] and the $\overline{\mathcal{W}}_l(q, \Delta E)$ functions defined here are related by

$$\overline{\mathcal{W}}_l(q, \Delta E) = 2\Delta E \sum_{n,\ell} \int \frac{\mathrm{d}k'}{k'} W_l^{n\ell}(k', q)\, \delta(\Delta E - E_{k'\ell'm'} + E_{n\ell m}) . \tag{3.18}$$

Since we are interested in the ionisation of isolated atoms, in eq. (3.18) $E_{k'\ell'm'} = k'^2/(2m_e)$ and the initial state energy, $E_{n\ell m}$, does not depend on m. Consequently, eq. (3.18) consistently gives a response function $\overline{\mathcal{W}}_l(q, \Delta E)$ that is independent of quantum numbers. Also, requiring that $v_{\min}(q, \Delta E)$ is less than the maximum speed a DM particle can have in the galaxy, $v_{\max} = v_e + v_{\mathrm{esc}}$, implies that only certain regions in the $(q, \Delta E)$ plane are kinematically allowed.

We conclude this subsection by providing an explicit relation between our response function $\overline{\mathcal{W}}_1$ and the standard ionisation form factor $f_{\mathrm{ion}}^{n\ell}$ used within the dark photon model, namely

$$\overline{\mathcal{W}}_1(q, \Delta E) = 2\Delta E \sum_{n,\ell} \int \frac{\mathrm{d}k'}{k'} |f_{\mathrm{ion}}^{n\ell}(k', q)|^2\, \delta(\Delta E - E_{k'\ell'm'} + E_{n\ell m}) . \tag{3.19}$$

In the numerical applications, we compute the response functions $W_l^{n\ell}(k', q)$ by using the DarkART code [53], which implements the equations we derived in [1].

3.1.2 Crystals

Similarly, in the case of crystal detectors such as SENSEI and EDELWEISS one can use eq. (3.12) with

$$\mathcal{W}_l(\boldsymbol{q}, \Delta E) = \frac{2}{\pi}\Delta E \sum_{ii'} \int_{\mathrm{BZ}} \frac{V\mathrm{d}^3 k}{(2\pi)^3} \int_{\mathrm{BZ}} \frac{V\mathrm{d}^3 k'}{(2\pi)^3} \mathscr{B}_l\, \delta(\Delta E - E_{i'\boldsymbol{k}'} + E_{i\boldsymbol{k}}) \tag{3.20}$$

to calculate the response functions $\overline{\mathcal{W}}_l(q, \Delta E)$. In this case, $r = 5$ functions $\mathscr{B}_l$ are non zero [2],

$$\mathscr{B}_1 = |f_{i\boldsymbol{k} \to i'\boldsymbol{k}'}|^2 \tag{3.21}$$

$$\mathscr{B}_2 = \frac{\boldsymbol{q}}{m_e} \cdot (f_{i\boldsymbol{k} \to i'\boldsymbol{k}'})(\boldsymbol{f}_{i\boldsymbol{k} \to i'\boldsymbol{k}'})^* \tag{3.22}$$

$$\mathscr{B}_3 = |\boldsymbol{f}_{i\boldsymbol{k} \to i'\boldsymbol{k}'}|^2 \tag{3.23}$$

$$\mathscr{B}_4 = \left| \frac{\boldsymbol{q}}{m_e} \cdot \boldsymbol{f}_{i\boldsymbol{k} \to i'\boldsymbol{k}'} \right|^2 \tag{3.24}$$

$$\mathscr{B}_5 = i\frac{\boldsymbol{q}}{m_e} \cdot [\boldsymbol{f}_{i\boldsymbol{k} \to i'\boldsymbol{k}'} \times (\boldsymbol{f}_{i\boldsymbol{k} \to i'\boldsymbol{k}'})^*] . \tag{3.25}$$

Interestingly, the response function induced by $\mathscr{B}_5$ is identically zero in the case of isolated atoms [1]. Here, $E_{i\boldsymbol{k}}$ ($E_{i'\boldsymbol{k}'}$) is the energy of the $i\boldsymbol{k}$ ($i'\boldsymbol{k}'$) initial state valence (final state conduction) electron, while $f_{1\to2}$ ($\boldsymbol{f}_{1\to2}$) is replaced by $f_{i\boldsymbol{k}}$ ($\boldsymbol{f}_{i'\boldsymbol{k}'}$), and $V = N_{\text{cell}}V_{\text{cell}}$, where V_{cell} is the volume of a unit cell, and N_{cell} the number of unit cells in the crystal. Note that the functions $\overline{\mathcal{W}}_l$ defined via eq. (3.20) and the functions $\overline{W}_l$ introduced in [2] are related as follows

$$\overline{\mathcal{W}}_l(q, \Delta E) = N_{\text{cell}}\,\overline{W}_l(q, \Delta E)\,. \tag{3.26}$$

By absorbing N_{cell} in the definition of $\overline{\mathcal{W}}_l$, eq. (3.9) applies to both isolated atoms and crystals. Finally, $\overline{\mathcal{W}}_1$ and the crystal form factor used in the dark photon model, f_{crystal}, are related by

$$\overline{\mathcal{W}}_1(q, \Delta E) = \frac{8\Delta E \alpha m_e^2 N_{\text{cell}}}{q^3}\,|f_{\text{crystal}}(q, \Delta E)|^2\;, \tag{3.27}$$

where α is the fine structure constant. In the numerical applications, we compute the response functions $\overline{W}_l(q, \Delta E)$ by using the QEdark-EFT code [54], which implements the equations we derived in [2].

3.1.3 Unified notation

Remarkably, the response functions $\mathcal{W}_l(\boldsymbol{q}, \Delta E)$ for isolated atoms, eq. (3.13), and those for crystals, eq. (3.20), have the very same form. Specifically, they can both be expressed as follows

$$\mathcal{W}_l(\boldsymbol{q}, \Delta E) = \frac{2}{\pi}\Delta E \sum_{\{1\},\{2\}} \mathscr{B}_l\,\delta(\Delta E - E_2 + E_1)\,, \tag{3.28}$$

where $\sum_{\{1\},\{2\}}$ represents the sums/integrals over all relevant physical states in eq. (3.13) and eq. (3.20). In the case of isolated atoms, eq. (3.28) gives the "detector response" for a single atom, whereas in the case of crystal detectors eq. (3.28) gives the "detector response" for a single crystal. In order to compare the two quantities, we introduce a *detector response per unit mass*,

$$\widetilde{\mathcal{W}}_l(q, \Delta E) \equiv \overline{\mathcal{W}}_l(q, \Delta E)/\widetilde{m}\,, \tag{3.29}$$

where for isolated atoms $\widetilde{m} = m_{\text{Xe}}$, m_{Xe} being the mass of a xenon atom, whereas for crystals, $\widetilde{m} = m_{\text{cell}}N_{\text{cell}}$, m_{cell} and N_{cell} being the mass and number of unit cells. Figure 1 shows the ratios

$$(\widetilde{\mathcal{W}}_l^{(\text{Xe})} - \widetilde{\mathcal{W}}_l^{(\text{Ge})})/(\widetilde{\mathcal{W}}_l^{(\text{Xe})} + \widetilde{\mathcal{W}}_l^{(\text{Ge})}) \tag{3.30}$$

and

$$(\widetilde{\mathcal{W}}_l^{(\text{Xe})} - \widetilde{\mathcal{W}}_l^{(\text{Si})})/(\widetilde{\mathcal{W}}_l^{(\text{Xe})} + \widetilde{\mathcal{W}}_l^{(\text{Si})}) \tag{3.31}$$

in the $(q, \Delta E)$ plane for $l = 1$ and $l = 2$. Similarly, figure 2 shows the same ratios now for $l = 3$ and $l = 4$. In both cases, a superscript specifies the material for which $\widetilde{\mathcal{W}}_l(q, \Delta E)$ is evaluated. Notice that only the regions above the black dashed lines are kinematically allowed in the two figures for our choice of v_{esc} and v_e. For larger v_{esc}, for example, smaller $|\boldsymbol{q}|$ would be accessible. As expected, for ΔE below the xenon ionisation threshold, $\widetilde{\mathcal{W}}_l^{(\text{Ge})}$ and $\widetilde{\mathcal{W}}_l^{(\text{Si})}$ dominate over $\widetilde{\mathcal{W}}_l^{(\text{Xe})}$, showing that xenon and crystal detectors are mainly sensitive to complementary regions in the $(q, \Delta E)$ plane. Despite this general trend, for deposited energies above about
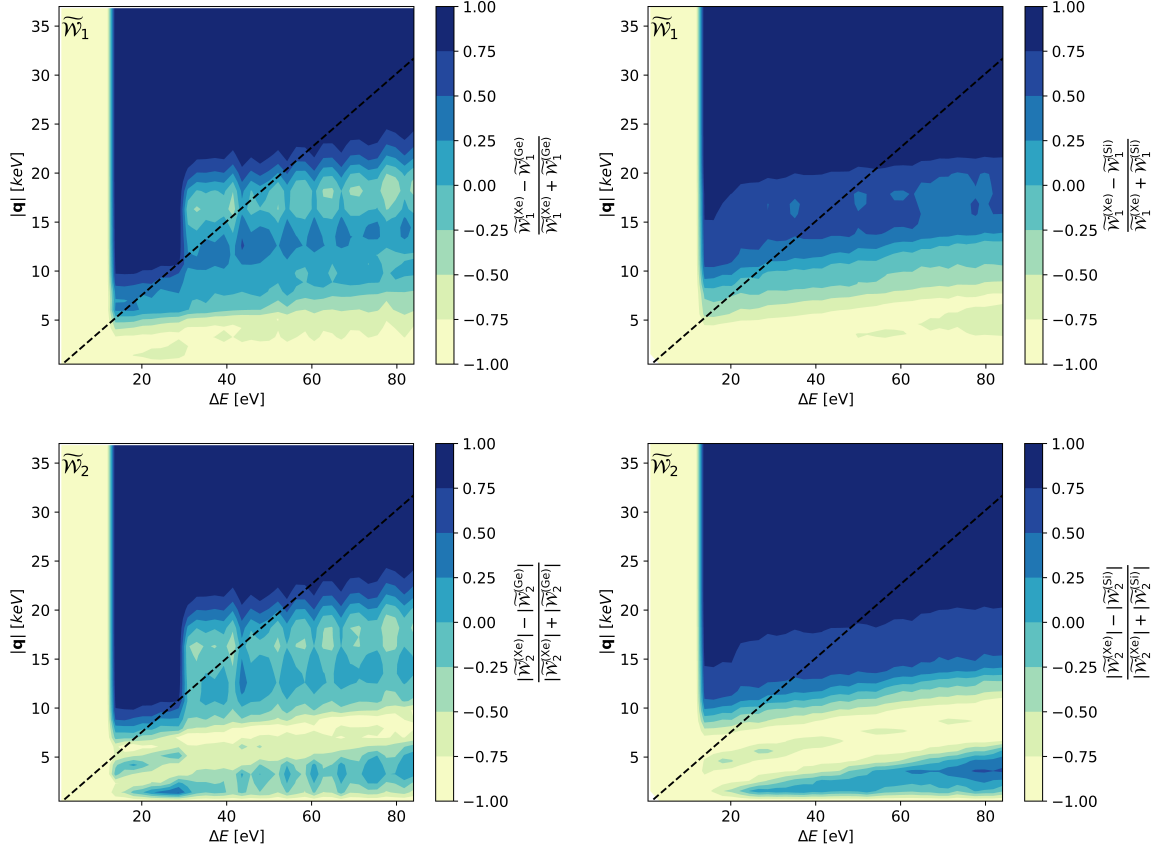
Figure 1. Relative differences between detector response functions per unit mass for xenon and germanium (left), and for xenon and silicon (right) detectors in the $(q, \Delta E)$ plane. The top (bottom) panels refer to $l = 1$ ($l = 2$). Regions above the black dashed line are kinematically allowed.

30 eV the germanium $3d$ bands contribute significantly to $\widetilde{\mathcal{W}}_l^{(\text{Ge})}$ and the ratio $\widetilde{\mathcal{W}}_l^{(\text{Ge})}/\widetilde{\mathcal{W}}_l^{(\text{Xe})}$ can be of the order of 1 for kinematically allowed values of the momentum transfer. While for $l = 1$, $l = 3$ and $l = 4$ the response function $\overline{\mathcal{W}}_l(q, \Delta E)$ is always real, for $l = 2$, we replace $\overline{\mathcal{W}}_2(q, \Delta E)$ with $|\overline{\mathcal{W}}_2(q, \Delta E)|$ in eqs. (3.30) and (3.31), as the former takes complex values for crystals. In the case of isolated atoms, all material response functions are real.

With the notation of eq. (3.28), we can also write a general relation between products of material and DM response functions, and the modulus squared of the transition amplitude, namely

$$\sum_{l=1}^{r} \text{Re}\left[\mathcal{R}_l^*(q, v)\overline{\mathcal{W}}_l(q, \Delta E)\right] = \frac{2}{\pi}\Delta E \sum_{\{1\},\{2\}} \int d\Omega_q \overline{\overline{|\mathcal{M}_{1\to 2}(\boldsymbol{v}, \boldsymbol{q})|^2}} \, \delta(\Delta E - E_2 + E_1), \quad (3.32)$$

where we used [2]

$$\overline{\overline{|\mathcal{M}_{1\to 2}(\boldsymbol{v}, \boldsymbol{q})|^2}} \equiv \frac{1}{2\pi}\int d\phi \, \overline{|\mathcal{M}_{1\to 2}(\boldsymbol{v}, \boldsymbol{q})|^2}_{\cos\theta=\xi}$$

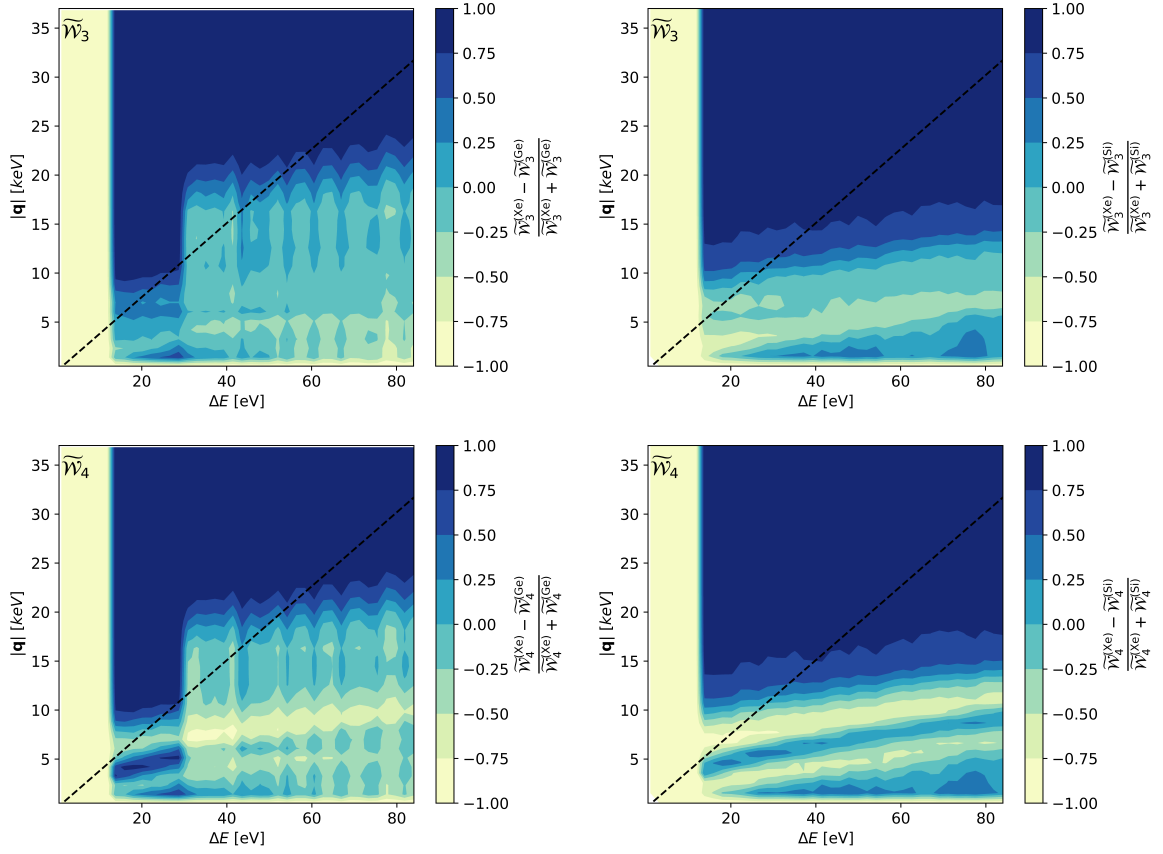$$= \sum_{l=1}^{r} \text{Re}\left[\mathcal{R}_l^*(q, v)\mathscr{B}_l(\boldsymbol{q})\right], \quad (3.33)$$

Figure 2. The same as for figure 1, now for $l = 3$ and $l = 4$.

θ and ϕ are polar and azimuthal angle of the velocity vector $\boldsymbol{v}$ in a frame with z-axis in the direction of $\boldsymbol{q}$,

$$\xi = \frac{q}{2m_{\mathrm{DM}}v} + \frac{\Delta E}{qv}, \tag{3.34}$$

and, finally, a single bar denotes a sum (average) over final (initial) DM/electron spin configurations. In the evaluation of the azimuthal average in eq. (3.33), we use the following identifies [2]

$$\frac{1}{2\pi} \int_0^{2\pi} \mathrm{d}\phi \, \boldsymbol{v}_{\mathrm{el}}^{\perp} \cdot \boldsymbol{A} \bigg|_{\cos\theta=\xi} = \frac{\boldsymbol{q}}{m_e} \cdot \boldsymbol{A} \left(\frac{|\boldsymbol{q}|}{m_e}\right)^{-2} \frac{\boldsymbol{q}}{m_e} \cdot \boldsymbol{v}_{\mathrm{el}}^{\perp}$$

$$\frac{1}{2\pi} \int_0^{2\pi} \mathrm{d}\phi \, \boldsymbol{v}_{\mathrm{el}}^{\perp} \cdot \left(\frac{\boldsymbol{q}}{m_e} \times \boldsymbol{A}\right) \bigg|_{\cos\theta=\xi} = 0, \tag{3.35}$$

where $\boldsymbol{A}$ is an arbitrary three-dimensional vector. We refer to [2] for a derivation of these equations. In our numerical applications, we will be interested in the non-relativistic limit of

$$\mathcal{O}_1 = \mathbb{1}_{\text{DM}}\mathbb{1}_e$$

$$\mathcal{O}_4 = \boldsymbol{S}_{\text{DM}} \cdot \boldsymbol{S}_e \qquad\qquad\qquad\qquad \mathcal{O}_{11} = i\boldsymbol{S}_{\text{DM}} \cdot \frac{\boldsymbol{q}}{m_e}\mathbb{1}_e$$

$$\mathcal{O}_5 = i\boldsymbol{S}_{\text{DM}} \cdot \left(\frac{\boldsymbol{q}}{m_e} \times \boldsymbol{v}^\perp\right)\mathbb{1}_e \qquad\qquad \mathcal{O}_{14} = i\left(\boldsymbol{S}_{\text{DM}} \cdot \frac{\boldsymbol{q}}{m_e}\right)\left(\boldsymbol{S}_e \cdot \boldsymbol{v}^\perp\right)$$

$$\mathcal{O}_6 = \left(\boldsymbol{S}_{\text{DM}} \cdot \frac{\boldsymbol{q}}{m_e}\right)\left(\boldsymbol{S}_e \cdot \frac{\boldsymbol{q}}{m_e}\right) \qquad\qquad \mathcal{O}_{15} = -\left(\boldsymbol{S}_{\text{DM}} \cdot \frac{\boldsymbol{q}}{m_e}\right)\left[\left(\boldsymbol{S}_e \times \boldsymbol{v}^\perp\right) \cdot \frac{\boldsymbol{q}}{m_e}\right]$$

$$\mathcal{O}_7 = \boldsymbol{S}_e \cdot \boldsymbol{v}^\perp \mathbb{1}_{\text{DM}} \qquad\qquad\qquad \mathcal{O}_{17} = i\frac{\boldsymbol{q}}{m_e} \cdot \boldsymbol{\mathcal{S}} \cdot \boldsymbol{v}^\perp \mathbb{1}_e$$

$$\mathcal{O}_8 = \boldsymbol{S}_{\text{DM}} \cdot \boldsymbol{v}^\perp \mathbb{1}_e \qquad\qquad\qquad \mathcal{O}_{18} = i\frac{\boldsymbol{q}}{m_e} \cdot \boldsymbol{\mathcal{S}} \cdot \boldsymbol{S}_e$$

$$\mathcal{O}_9 = i\boldsymbol{S}_{\text{DM}} \cdot \left(\boldsymbol{S}_e \times \frac{\boldsymbol{q}}{m_e}\right) \qquad\qquad \mathcal{O}_{19} = \frac{\boldsymbol{q}}{m_e} \cdot \boldsymbol{\mathcal{S}} \cdot \frac{\boldsymbol{q}}{m_e}\mathbb{1}_e$$

$$\mathcal{O}_{10} = i\boldsymbol{S}_e \cdot \frac{\boldsymbol{q}}{m_e}\mathbb{1}_{\text{DM}} \qquad\qquad\qquad \mathcal{O}_{20} = \left(\boldsymbol{S}_e \times \frac{\boldsymbol{q}}{m_e}\right) \cdot \boldsymbol{\mathcal{S}} \cdot \frac{\boldsymbol{q}}{m_e}$$

Table 1. List of operators that can contribute to the transition amplitude for the models considered here. We denote by $\mathbb{1}_{\text{DM}}$ ($\mathbb{1}_e$) the identity in the DM (electron) spin space. Similarly, $\boldsymbol{S}_{\text{DM}}$ ($\boldsymbol{S}_e$) is the DM (electron) spin operator. For spin-0 DM, $\langle\boldsymbol{S}_{\text{DM}}\rangle = 0$. For spin-1/2 DM $\langle\boldsymbol{S}_{\text{DM}}\rangle = \delta^{r'r}\xi^{s'}\boldsymbol{\sigma}\xi^s/2$, where r (s) labels the initial electron (DM) spin configuration, r' (s') identifies the final electron (DM) spin configuration and $\boldsymbol{\sigma} = (\sigma_1, \sigma_2, \sigma_3)$ consists of the three Pauli matrices. For spin-1 DM, $\langle\boldsymbol{S}_{\text{DM}}\rangle = -i\delta^{r'r}\boldsymbol{e}'_{s'} \times \boldsymbol{e}_s$, where $\boldsymbol{e}_s$ and $\boldsymbol{e}'_{s'}$ are three-dimensional polarisation vectors. Finally, $\langle\boldsymbol{\mathcal{S}}\rangle = \delta^{r'r}(e_{si}e'_{s'j} + e_{sj}e'_{s'i})/2$. See appendix B for further details.

eq. (3.33),

$$\overline{|\mathcal{M}_{1\to 2}(\boldsymbol{v}, \boldsymbol{q})|^2} \simeq \overline{|\mathcal{M}(\boldsymbol{q}, \boldsymbol{v}^\perp_{\text{el}})|^2_{\boldsymbol{\ell}=\boldsymbol{0}}|f_{1\to 2}(\boldsymbol{q})|^2}$$

$$+ 2m_e\text{Re}\left[\overline{\mathcal{M}(\boldsymbol{q}, \boldsymbol{v}^\perp_{\text{el}})_{\boldsymbol{\ell}=0}f_{1\to 2}(\boldsymbol{q})[\nabla_{\boldsymbol{\ell}}\mathcal{M}^*(\boldsymbol{q}, \boldsymbol{v}^\perp_{\text{el}})]_{\boldsymbol{\ell}=0} \cdot \boldsymbol{f}^*_{1\to 2}(\boldsymbol{q})}\right]$$

$$+ m_e^2\overline{|[\nabla_{\boldsymbol{\ell}}\mathcal{M}(\boldsymbol{q}, \boldsymbol{v}^\perp_{\text{el}})]_{\boldsymbol{\ell}=0} \cdot \boldsymbol{f}_{1\to 2}(\boldsymbol{q})|^2}\,. \tag{3.36}$$

3.2 Tree-level application to specific models

In this section, we calculate the DM response functions $\mathcal{R}_l(q, v)$ associated with the models for DM-electron interactions of section 2. We refer to appendix A for a detailed account of these calculations.

3.2.1 Scalar dark matter

In the case of *scalar DM with a scalar mediator*, the free amplitude for DM-electron scattering is

$$i\mathcal{M} = ig_1 m_S\left[\frac{i}{(k'-k)^2 - m_\phi^2}\right]\left[\overline{u}^{r'}(k')i(h_1 + ih_2\gamma^5)u^r(k)\right]\,, \tag{3.37}$$

where $u^r(k)$, $r = 1, 2$ and $\overline{u}^{r'}(k')$, $r' = 1, 2$ are free Dirac spinors for the initial and final state electron, while k and k' are four-momenta. In the non-relativistic limit, eq. (3.37) can be written as

$$i\mathcal{M} \simeq i2m_S m_e\left(\frac{g_1 h_1}{|\boldsymbol{q}|^2 + m_\phi^2}\langle\hat{\mathcal{O}}_1\rangle - \frac{g_1 h_2}{|\boldsymbol{q}|^2 + m_\phi^2}\langle\hat{\mathcal{O}}_{10}\rangle\right)\,, \tag{3.38}$$

where the operators $\hat{\mathcal{O}}_1$ and $\hat{\mathcal{O}}_{10}$ are given in table 1, and angle brackets in general denote an expectation value between initial, s/r, and final, s'/r', DM/electron spin configurations. For example, $\langle \hat{\mathcal{O}}_1 \rangle = \delta^{r'r}\delta^{s's}$. For scalar DM $\delta^{s's} \to 1$, while $s, s' = 1, 2$ ($s, s' = 1, 2, 3$) for spin-1/2 (spin-1) DM. By inserting eq. (3.38) into eq. (3.4), we find the modulus squared transition amplitude

$$\overline{|M_{1\to2}|^2} = \left(c_1^2 + \frac{1}{4}c_{10}^2 \frac{|\boldsymbol{q}|^2}{m_e^2} \right) \mathscr{B}_1 \, , \tag{3.39}$$

where the coupling constants c_1 and c_{10} are related to the coupling constants and masses of the underlying model as in table 2. Notice the $1/\Gamma(u,t)$ factor in the definition of c_1 and c_{10}, where

$$\Gamma(u,t)^{-1} \equiv 4t(1+u^2)^{-1} \, , \tag{3.40}$$

arising from the mediator propagator. Comparing eq. (3.39) with the second line in eq. (3.33), we find

$$\mathcal{R}_1(q,v) = \left(c_1^2 + \frac{1}{4}c_{10}^2 \frac{|\boldsymbol{q}|^2}{m_e^2} \right) \, , \tag{3.41}$$

while $\mathcal{R}_2(q,v) = \mathcal{R}_3(q,v) = \mathcal{R}_4(q,v) = \mathcal{R}_5(q,v) = 0$. The case of spin 0 DM with a scalar mediator is thus not characterised by new features, since the observable electron transition rate can in this case be computed by using the response function $\overline{\mathcal{W}}_1$, as in the dark photon model.

As a first non trivial example where the ionisation and crystal form factors commonly used in the case of the dark photon model provide a poor description of the rate of electron transitions induced by DM scattering, let us consider the case of *scalar DM with a vector mediator*. For this model, the free amplitude for DM-electron scattering can be written as follows

$$i\mathcal{M} = ig_4 P_\mu \left[\frac{-ig^{\mu\nu}}{(k'-k)^2 - m_G^2} \right] \left[\overline{u}^{r'}(k')i(h_3\gamma_\nu + ih_4\gamma_\nu\gamma^5)u^r(k) \right] \, , \tag{3.42}$$

where $P = p + p'$, and p (p') is the initial (final) DM four-momentum. In the non-relativistic limit,

$$i\mathcal{M} \simeq i2m_S m_e \left(-\frac{2g_4 h_3}{|\boldsymbol{q}|^2 + m_G^2}\langle \hat{\mathcal{O}}_1 \rangle + \frac{4g_4 h_4}{|\boldsymbol{q}|^2 + m_G^2}\langle \hat{\mathcal{O}}_7 \rangle \right) \, , \tag{3.43}$$

where the operators $\hat{\mathcal{O}}_1$ and $\hat{\mathcal{O}}_7$ are listed in table 1. For the azimuthal average of the squared modulus of the transition amplitude $\mathcal{M}_{1\to2}$ (defined in eq. (3.33) and used in eq. (3.32)), we now find

$$\overline{\overline{|\mathcal{M}_{1\to2}(\boldsymbol{v},\boldsymbol{q})|^2}} = \left(c_1^2 + \frac{1}{4}c_7^2 |\boldsymbol{v}_{\text{el}}^\perp|^2 \right) \mathscr{B}_1 - \frac{1}{2}c_7^2 \left(\frac{\boldsymbol{q}}{m_e} \cdot \boldsymbol{v}_{\text{el}}^\perp \right) \frac{m_e^2}{|\boldsymbol{q}|^2} \mathscr{B}_2 + \frac{1}{4}c_7^2 \mathscr{B}_3 \, , \tag{3.44}$$

which implies

$$\begin{aligned}
\mathcal{R}_1(q,v) &= \left(c_1^2 + \frac{1}{4}c_7^2 |\boldsymbol{v}_{\text{el}}^\perp|^2 \right) \\
\mathcal{R}_2(q,v) &= -\frac{1}{2}c_7^2 \left(\frac{\boldsymbol{q}}{m_e} \cdot \boldsymbol{v}_{\text{el}}^\perp \right) \frac{m_e^2}{|\boldsymbol{q}|^2} \\
\mathcal{R}_3(q,v) &= \frac{1}{4}c_7^2 \, ,
\end{aligned} \tag{3.45}$$

Scalar Mediator, $u = \|\boldsymbol{q}\|/m_\phi,\ t = m_S m_e/m_\phi^2$		Vector Mediator, $u = \|\boldsymbol{q}\|/m_G,\ t = m_S m_e/m_G^2$	
$c_1 = \dfrac{1}{2}\dfrac{g_1 h_1}{\Gamma(u,t)}$	$c_{10} = -\dfrac{1}{2}\dfrac{g_1 h_2}{\Gamma(u,t)}$	$c_1 = -\dfrac{g_4 h_3}{\Gamma(u,t)}$	$c_7 = \dfrac{2 g_4 h_4}{\Gamma(u,t)}$

Table 2. Relation between the coupling constants in the Lagrangians of eq. (2.1) and eq. (2.2), and the non-relativistic coupling constants in the DM response functions for, respectively, scalar DM with a scalar mediator, eq. (3.41), and scalar DM with a vector mediator, eq. (3.45). The dimensionless function $\Gamma(u,t)^{-1} \equiv 4t(1+u^2)^{-1}$ accounts for the dependence of the non-relativistic coupling constants on the momentum transfer $\boldsymbol{q}$ and the mediator mass, m_ϕ or m_G.

with $\mathcal{R}_4(q,v) = \mathcal{R}_5(q,v) = 0$. Table 2 relates c_1 and c_7 to the parameters of the underling DM model. As in the previous example, in table 2 we include a $1/\Gamma(u,t)$ factor in the definition of c_1 and c_7.

3.2.2 Fermionic dark matter

The calculation of the DM response functions $\mathcal{R}_l(q,v)$ for fermionic DM proceeds as in the case of spin-0 DM, which we discussed in detail in the previous subsection. We provide the details of such a calculation in appendix A and appendix B. Here, we limit ourselves to listing the final results, placing the emphasis on models that predict material responses different from the standard ionisation and crystal form factors. For *fermionic DM with a scalar mediator*, we find

$$\mathcal{R}_1(q,v) = c_1^2 + \frac{1}{16}c_6^2\frac{|\boldsymbol{q}|^4}{m_e^4} + \frac{1}{4}c_{10}^2\frac{|\boldsymbol{q}|^2}{m_e^2} + \frac{1}{4}c_{11}^2\frac{|\boldsymbol{q}|^2}{m_e^2}\,, \tag{3.46}$$

while $\mathcal{R}_2(q,v) = \mathcal{R}_3(q,v) = \mathcal{R}_4(q,v) = \mathcal{R}_5(q,v) = 0$. As in the case of spin-0 DM with a scalar mediator (see eq. (3.41)), we find that in a scenario where DM is made of spin-1/2 particles interacting with electrons through the exchange of a scalar mediator particle the standard ionisation and crystal form factors can properly describe the response of materials to an external DM perturbation. In contrast, for *fermionic DM with a vector mediator*, we find

$$\mathcal{R}_1(q,v) = c_1^2 + \frac{3}{16}c_4^2 + \frac{1}{4}c_7^2|\boldsymbol{v}_{\mathrm{el}}^\perp|^2 + \frac{1}{4}c_8^2|\boldsymbol{v}_{\mathrm{el}}^\perp|^2 + \frac{1}{8}c_9^2\frac{|\boldsymbol{q}|^2}{m_e^2}$$

$$\mathcal{R}_2(q,v) = -\left(\frac{\boldsymbol{q}}{m_e}\cdot\boldsymbol{v}_{\mathrm{el}}^\perp\right)\frac{m_e^2}{|\boldsymbol{q}|^2}\left(\frac{1}{2}c_7^2 + \frac{1}{2}c_8^2\right)$$

$$\mathcal{R}_3(q,v) = \frac{1}{4}c_7^2 + \frac{1}{4}c_8^2\,, \tag{3.47}$$

$\mathcal{R}_4(q,v) = \mathcal{R}_5(q,v) = 0$. We therefore conclude that it is crucial to evaluate the material response functions $\overline{\mathcal{W}}_2(q,\Delta E)$ and $\overline{\mathcal{W}}_3(q,\Delta E)$, in addition to the standard ionisation and crystal form factors, to consistently compare theoretical predictions with experimental data in a model with fermionic DM and a vector mediator. For example, neglecting the $\overline{\mathcal{W}}_2(q,\Delta E)$ and $\overline{\mathcal{W}}_3(q,\Delta E)$ response functions when computing an exclusion limit from a null result, or when interpreting a signal at a DM direct detection experiment, would lead to strongly biased results if nature is indeed described by fermionic DM with a vector mediator.

Scalar Mediator,		Vector Mediator,	
$u = \|\boldsymbol{q}\|/m_\phi,\ t = m_\chi m_e/m_\phi^2$		$u = \|\boldsymbol{q}\|/m_G,\ t = m_\chi m_e/m_G^2$	
$c_1 = \dfrac{\lambda_1 h_1}{\Gamma(u,t)}$ $\qquad c_6 = \dfrac{\lambda_2 h_2}{\Gamma(u,t)}\dfrac{m_e}{m_\chi}$		$c_1 = -\dfrac{\lambda_3 h_3}{\Gamma(u,t)}$ $\qquad c_4 = \dfrac{4\lambda_4 h_4}{\Gamma(u,t)}$	
$c_{10} = -\dfrac{\lambda_1 h_2}{\Gamma(u,t)}$ $\qquad c_{11} = \dfrac{\lambda_2 h_1}{\Gamma(u,t)}\dfrac{m_e}{m_\chi}$		$c_7 = \dfrac{2\lambda_3 h_4}{\Gamma(u,t)}$ $\qquad c_8 = -\dfrac{2\lambda_4 h_3}{\Gamma(u,t)}$	
		$c_9 = \dfrac{2\lambda_3 h_4}{\Gamma(u,t)}\dfrac{m_e}{m_\chi} + \dfrac{2\lambda_4 h_3}{\Gamma(u,t)}$	

Table 3. Relation between the coupling constants in the Lagrangians of eq. (2.3) and eq. (2.4) and the non-relativistic coupling constants in the DM response functions for, respectively, fermionic DM with a scalar mediator, eq. (3.46), and fermionic DM with a vector mediator, eq. (3.47). Here, we introduced the dimensionless function $\Gamma(u,t)^{-1} \equiv 4t(1+u^2)^{-1}$ to account for the dependence of the non-relativistic coupling constants on $\boldsymbol{q}$ and the mediator mass.

3.2.3 Vector dark matter

In the case of *spin-1 DM with a scalar mediator* we find that just a single response function contributes to the observed rate of electron transitions induced by DM scattering in a material, namely

$$\mathcal{R}_1(q,v) = c_1^2 + \frac{1}{4}c_{10}^2\frac{|\boldsymbol{q}|^2}{m_e^2}\,, \tag{3.48}$$

while $\mathcal{R}_2(q,v) = \mathcal{R}_3(q,v) = \mathcal{R}_4(q,v) = \mathcal{R}_5(q,v) = 0$. We therefore find that in all models where the interaction between DM and the electrons bound to a material is mediated by the exchange of a scalar mediator the rate of DM-induced electron transitions can be computed by using the standard ionisation and crystal form factors. Turning this argument around, we find that experimental evidence for contributions to the theoretical rate $\mathscr{R}_{\text{theory}}$ from $\mathcal{W}_l$, with $l \neq 1$, would point towards DM-electron interactions mediated by particles with spin different from zero.

The case of *spin-1 DM with a vector mediator* exhibits a richer phenomenology, with several material response functions possibly contributing to the theoretical rate $\mathscr{R}_{\text{theory}}$. Specifically,

$$\mathcal{R}_1(q,v) = c_1^2 + \frac{1}{2}c_4^2 + \frac{2}{3}c_5^2\left|\frac{\boldsymbol{q}}{m_e}\times\boldsymbol{v}_{\text{el}}^\perp\right|^2 + \frac{1}{6}c_6^2\frac{|\boldsymbol{q}|^4}{m_e^4} + \frac{1}{4}c_7^2|\boldsymbol{v}_{\text{el}}^\perp|^2 + \frac{2}{3}c_8^2|\boldsymbol{v}_{\text{el}}^\perp|^2$$
$$+ \frac{1}{3}c_9^2\frac{|\boldsymbol{q}|^2}{m_e^2} + \frac{2}{3}c_{11}^2\frac{|\boldsymbol{q}|^2}{m_e^2} + \frac{1}{6}c_{14}^2|\boldsymbol{v}_{\text{el}}^\perp|^2\frac{|\boldsymbol{q}|^2}{m_e^2}$$
$$+ \frac{1}{6}c_{17}^2\left(\left|\frac{\boldsymbol{q}}{m_e}\cdot\boldsymbol{v}_{\text{el}}^\perp\right|^2 + \frac{|\boldsymbol{q}|^2}{m_e^2}|\boldsymbol{v}_{\text{el}}^\perp|^2\right) + \frac{1}{6}c_{18}^2\frac{|\boldsymbol{q}|^2}{m_e^2} + \frac{1}{3}c_{19}^2\frac{|\boldsymbol{q}|^4}{m_e^4}$$
$$+ \frac{1}{12}c_{20}^2\frac{|\boldsymbol{q}|^4}{m_e^4} + \frac{1}{3}c_4 c_6\frac{|\boldsymbol{q}|^2}{m_e^2} + \frac{2}{3}c_1 c_{19}\frac{|\boldsymbol{q}|^2}{m_e^2}$$
$$\text{Re}[\mathcal{R}_2(v,q)] = -\left(\frac{\boldsymbol{q}}{m_e}\cdot\boldsymbol{v}_{\text{el}}^\perp\right)\left[\frac{m_e^2}{|\boldsymbol{q}|^2}\left(\frac{1}{2}c_7^2 + \frac{4}{3}c_8^2\right) + \frac{1}{3}c_{14}^2 + \frac{2}{3}c_{17}^2\right]$$
$$\text{Im}[\mathcal{R}_2(v,q)] = \frac{1}{2}c_7 c_{10} - \frac{1}{3}c_4 c_{14} + \frac{4}{3}c_8 c_{11} - \frac{1}{3}c_6 c_{14}\frac{|\boldsymbol{q}|^2}{m_e^2}$$

Scalar Mediator, $u = |\boldsymbol{q}|/m_\phi$, $t = m_X m_e/m_\phi^2$	
$c_1 = \dfrac{1}{2}\dfrac{b_1 h_1}{\Gamma(u,t)}$	$c_{10} = -\dfrac{1}{2}\dfrac{b_1 h_2}{\Gamma(u,t)}$

Vector Mediator, $u = |\boldsymbol{q}|/m_G$, $t = m_X m_e/m_G^2$	
$c_1 = -\dfrac{b_5 h_3}{\Gamma(u,t)}$	
$c_4 = \dfrac{\mathrm{Im}(b_6)h_3}{\Gamma(u,t)}\dfrac{m_e}{2m_X}\dfrac{|\boldsymbol{q}|^2}{m_e^2} - \dfrac{2\mathrm{Re}(b_7)h_4}{\Gamma(u,t)}$	$c_{11} = \dfrac{\mathrm{Im}(b_7)h_3}{\Gamma(u,t)}\dfrac{m_e}{2m_X}$
$c_5 = \dfrac{\mathrm{Im}(b_6)h_3}{\Gamma(u,t)}\dfrac{m_e}{2m_X}$	$c_{14} = -\dfrac{\mathrm{Im}(b_7)h_4}{\Gamma(u,t)}\dfrac{m_e}{m_X}$
$c_6 = -\dfrac{\mathrm{Im}(b_6)h_3}{\Gamma(u,t)}\dfrac{m_e}{2m_X}$	$c_{17} = -\dfrac{\mathrm{Re}(b_6)h_3}{\Gamma(u,t)}\dfrac{m_e}{m_X}$
$c_7 = \dfrac{2b_5 h_4}{\Gamma(u,t)}$	$c_{18} = \dfrac{2\mathrm{Re}(b_6)h_4}{\Gamma(u,t)}\dfrac{m_e}{m_X}$
$c_8 = \dfrac{\mathrm{Re}(b_7)h_3}{\Gamma(u,t)}$	$c_{19} = \dfrac{\mathrm{Im}(b_6)h_3}{\Gamma(u,t)}\dfrac{m_e^2}{2m_X^2}$
$c_9 = \dfrac{\mathrm{Im}(b_6)h_4}{\Gamma(u,t)}\dfrac{m_e}{m_X} - \dfrac{\mathrm{Re}(b_7)h_3}{\Gamma(u,t)}$	$c_{20} = -\dfrac{\mathrm{Re}(b_6)h_3}{\Gamma(u,t)}\dfrac{m_e}{m_X} - \dfrac{\mathrm{Im}(b_7)h_4}{\Gamma(u,t)}\dfrac{m_e^2}{m_X^2}$

Table 4. The same as in table 2 and table 3, now for vecto. DM.

$$\mathcal{R}_3(v,q) = \frac{1}{4}c_7^2 + \frac{2}{3}c_8^2 + \frac{|\boldsymbol{q}|^2}{m_e^2}\left(\frac{2}{3}c_5^2 + \frac{1}{6}c_{14}^2 + \frac{1}{6}c_{17}^2\right)$$
$$\mathcal{R}_4(v,q) = -\frac{2}{3}c_5^2 + \frac{1}{6}c_{17}^2\,, \tag{3.49}$$

with $R_5(q,v) = 0$. We refer to appendix A and appendix B for all details underling the derivation of eq. (3.49). Interestingly, none of the models considered here can generate the response function $\overline{\mathcal{W}}_5$.

3.3 One-loop application to specific models

So far, we focused on DM-electron interactions arising at tree level. These required a cubic DM-DM-mediator interaction vertex in the Lagragian. It is interesting to note that even when such cubic vertices are absent at tree level, DM-electron interactions can be generated at the one-loop level via a quartic DM-DM-mediator-mediator vertex, as shown in figure 3 in four specific cases: 1) scalar DM with a scalar mediator, 2) scalar DM with a vector mediator, 3) vector DM with a scalar mediator, and, finally 4) vector DM with a vector mediator. In appendix C, we list the free electron amplitude for the four diagrams in figure 3. They are all proportional to $\langle \hat{\mathcal{O}}_1 \rangle$, and therefore contribute to the observable rate of electron transitions induced by DM scattering in a detector material, $\mathscr{R}_{\text{theory}}$, via the response function $\overline{\mathcal{W}}_1(q, \Delta E)$ only. From the point of view of material physics and for the purposes of our work, this family of DM-electron interaction models is therefore equivalent to the dark photon model. In addition to the four loop diagrams in figure 3, one could also write down additional diagrams where the vertices of the external electron lines are swapped. Also in this case, one would
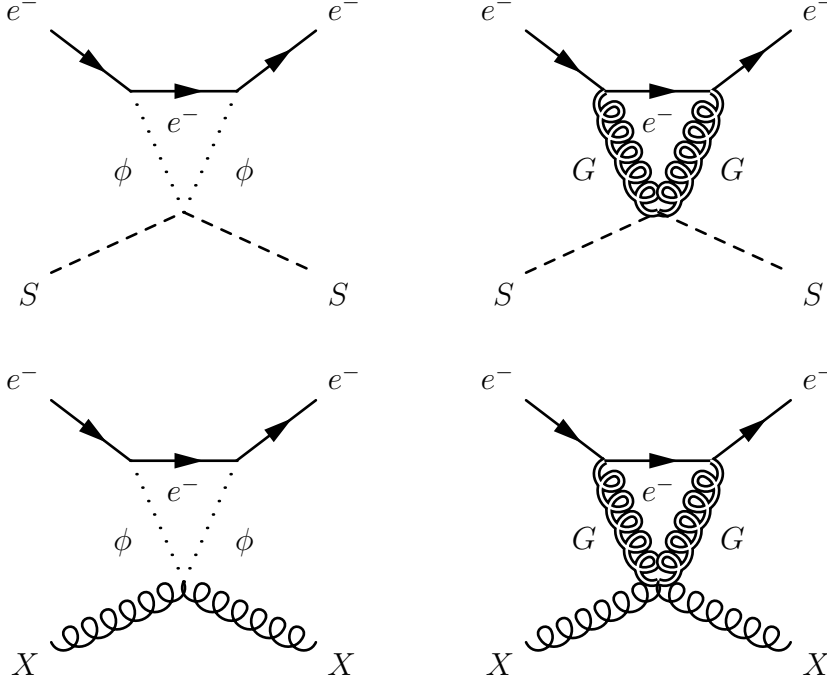
Figure 3. One-loop Feynman diagrams for DM-electron scattering assuming: 1) spin-0 DM with a scalar mediator (top left), 2) spin-0 DM with a vector mediator (top right), 3) spin-1 DM with a scalar mediator (bottom left) and, finally, 4) spin-1 DM with a vector mediator (bottom right). The particles in the processes are denoted by the letters used for the associated fields.

find that the associated amplitude is proportional to $\langle \hat{\mathcal{O}}_1 \rangle$ in the non-relativistic limit. For these reasons, here we do not investigate the effects of loop-induced DM-electron interactions any further.

4 Comparison with experimental data

In this section, we compare the rate of electron transitions predicted from the models of section 2 with experimental data released by the XENON10 [46], XENON1T [15], EDEL-WEISS [23] and SENSEI [24] collaborations. As we will see below, for xenon experiments we adopt the data analysis strategies we used in [1]. For the analysis of results from crystal detectors, we rely on [2].

4.1 Direct detection data

The XENON10 and XENON1T experiments are dual phase time projection chambers (TPCs) filled with liquid and gaseous xenon. They have been searching for sub-GeV DM particles in events where xenon atoms are ionised by DM-electron scattering in the liquid xenon detector component. In each such event, primary electrons from the ionised atoms are expected to propagate in the liquid xenon, producing a number n_e of secondary electrons. These secondary electrons are then extracted from the liquid target by means of an external electric field, and drifted into the gaseous xenon detector component, where they eventually generate a scintillation signal. This signal is finally recorded by photomultiplier tubes through the observation of S2 associated photoelectrons [15, 46]. Since S2 is the actually observed quantity

XENON10		XENON1T	
bin [S2]	observed events	bin [S2]	observed events
[14,41)	126	[150,200)	8
[41,68)	60	[200,250)	7
[68,95)	12	[250,300)	2
[95,122)	3	[300,350)	1
[122,149)	2	—	—
[149,176)	0	—	—
[176,203)	2	—	—

Table 5. Events in selected S2 bins observed by XENON10 [46] (left) and XENON1T [15] (right).

in xenon TPCs experiments, we need to rewrite our theoretical rate, eq. (3.9), as a function of S2.

Let us denote by $\mathscr{P}(n_e|E_e)$ the probability density to produce n_e secondary electrons in a DM-electron scattering event when the energy of the primary electron is $E_e = k'^2/(2m_e)$. Furthermore, let $\mathscr{P}(\text{S2}|n_e)$ be the probability density to observe S2 photoelectrons when n_e electrons drifted from the liquid xenon target into the gaseous phase. Then, the rate of DM-electron scattering events with a number of observed photoelectrons between S2 and $\text{S2} + d\text{S2}$ is [1]

$$d\mathscr{R}_{\text{obs}} = d\text{S2}\,\varepsilon(\text{S2})\frac{n_{\text{DM}}}{128\pi m_{\text{DM}}^2 m_e^2} \int d(\ln \Delta E) \int dq\, q\, \hat{\eta}(q, \Delta E) \sum_{n_e=1}^{\infty} \mathscr{P}(\text{S2}|n_e)$$
$$\times \sum_{l=1}^{r} \text{Re}\left[\mathcal{R}_l^*(q, v)\overline{\mathcal{W}}_l(q, \Delta E; n_e) \right], \tag{4.1}$$

where $\varepsilon(\text{S2})$ is the experiment-specific detection efficiency, and we introduced the modified response

$$\overline{\mathcal{W}}_l(q, \Delta E; n_e) \equiv \int d\Omega_q\, \mathcal{W}_l(\boldsymbol{q}, \Delta E; n_e), \tag{4.2}$$

with

$$\mathcal{W}_l(\boldsymbol{q}, \Delta E; n_e) = \frac{2}{\pi}\Delta E \sum_{n,\ell,m} \sum_{\ell',m'} \int \frac{V k'^2\, dk'}{(2\pi)^3}\, \mathscr{B}_l\, \mathscr{P}(n_e|E_e)\, \delta(\Delta E - E_{n\ell m} + E_{k'\ell'm'}). \tag{4.3}$$

It is important to note that eq. (4.1) gives the rate of observable events per atom in the detector, not the total rate. The total rate of observable events per unit detector mass is found by multiplying eq. (4.1) by the number of xenon atoms in the detector, n_{Xe}, and then dividing by the detector mass, $M_{\text{det}} = n_{\text{Xe}} m_{\text{Xe}}$, where m_{Xe} is the mass of a xenon atom. One finds,

$$d\widetilde{\mathscr{R}}_{\text{atoms}} \equiv d\mathscr{R}_{\text{obs}}/m_{\text{Xe}}. \tag{4.4}$$

We refer to [1] for further details on $\mathscr{P}(n_e|E_e)$, $\mathscr{P}(\text{S2}|n_e)$ and $\varepsilon(\text{S2})$. By integrating eq. (4.4) over the S2 bins in table 5, and multiplying the result by the experimental exposure (15

EDELWEISS		
[Q]	obs. events	exp. [g-day]
1	5814	3.23
2	44706	17.76
3	2718	80.72
4	227	80.72

SENSEI		
[Q]	obs. events	exp. [g-day]
1	758	1.38
2	5	2.09
3	0	9.03
4	0	9.10

Table 6. Events corresponding to $Q = 1, 2, 3, 4$ observed by the EDELWEISS [23] and SENSEI [24] experiments, together with the associated Q dependent effective exposure expressed in [g-day].

kg days for XENON10 and 80755 kg days for XENON1T), we obtain the expected number of DM signal events in the given S2 bin. We can then use the statistical methods reviewed below to compare our predictions with the XENON10 [46] and XENON1T [15] results we report in table 5.

A second class of experiments of interest for this work includes EDELWEISS [23] and SENSEI [24]. These experiments operate, respectively, germanium and silicon crystal detectors, and search for sub-GeV DM particles in events associated with the production of electron-hole pairs resulting from electronic transitions induced by DM-electron scattering in the detector crystals. In order to compare our theoretical rate, eq. (3.9), with EDELWEISS [23] and SENSEI [24] results, we first calculate the total event rate per unit detector mass by dividing eq. (3.9) by the detector mass, $m_{\text{det}} = N_{\text{cell}} m_{\text{cell}}$, where m_{cell} is the mass of a unit cell,

$$\mathrm{d}\widetilde{\mathscr{R}}_{\text{crystals}} \equiv \mathrm{d}\mathscr{R}_{\text{theory}}/m_{\text{det}} \,, \tag{4.5}$$

and then convert the deposited energy ΔE in eq. (4.5) into a number of electron-hole pairs produced in a DM-electron scattering event, which we denote by Q. We convert ΔE into Q using [18]

$$Q(\Delta E) = 1 + \lfloor (\Delta E - E_{\text{gap}})/\varepsilon \rfloor \,, \tag{4.6}$$

where $\lfloor \cdot \rfloor$ is the floor function. The observed band-gap and mean energy per electron-hole pair are $E_{\text{gap}} = 0.67 \,\text{eV}$ and $\varepsilon = 3.0 \,\text{eV}$ for germanium [23], and $E_{\text{gap}} = 1.20 \,\text{eV}$ and $\varepsilon = 3.8 \,\text{eV}$ for silicon [24]. We can then calculate the expected number of DM signal events corresponding to $Q = n$ electron-hole pairs, where $n \in \mathbb{N}$, by performing the ΔE integral in eq. (3.9) over the interval $[E_{\text{gap}} + (n - 1)\varepsilon, E_{\text{gap}} + n\varepsilon)$, and multiplying the result by the Q dependent effective exposure (that is, the exposure times the detection efficiency). We report the latter, together with the events actually observed by the EDELWEISS [23] and SENSEI [24] experiments in table 6.

Let us now denote by $\mathcal{S}_i$ the expected number of DM signal events in the i-th S2 bin, for XENON10 and XENON1T, or in the i-th Q bin, for EDELWEISS and SENSEI. Furthermore, let $\mathcal{D}_i$ be the number of actually observed events in the same (S2 or Q) bin. For each of the four experiments considered here, we calculate 90% confidence level (C.L.) exclusion limits on the strength of a given DM-electron interaction by requiring that $S_i \leq S_i^{90\%}$ for all bins, where

$$\sum_{k=\mathcal{D}_i+1}^{\infty} \mathcal{P}(k \,|\, \mathcal{S}_i^{90\%}) = 0.9 \tag{4.7}$$

Simplified models and underlying Lorentz structures	
Lagrangian	Lorentz structure
$\mathcal{L}_{g_4 h_4}^{(0)} = -ig_4(S^\dagger \partial_\mu S - \partial_\mu S^\dagger S)G^\mu - h_4(\overline{e}\gamma_\mu \gamma^5 e)G^\mu$	$\partial_- \otimes A$
$\mathcal{L}_{\lambda_3 h_4}^{(1/2)} = -\lambda_3 \overline{\chi}\gamma^\mu \chi G_\mu - h_4 \overline{e}\gamma_\mu \gamma^5 e G^\mu$	$V \otimes A$
$\mathcal{L}_{\lambda_4 h_3}^{(1/2)} = -\lambda_4 \overline{\chi}\gamma^\mu \gamma^5 \chi G_\mu - h_3 \overline{e}\gamma_\mu e G^\mu$	$A \otimes V$
$\mathcal{L}_{b_5 h_4}^{(1)} = -ib_5 \left[X_\nu^\dagger \partial_\mu X^\nu - (\partial_\mu X^{\dagger \nu})X_\nu \right] G^\mu - h_4 G_\mu \overline{e}\gamma^\mu \gamma^5 e$	$\partial_- \otimes A$
$\mathcal{L}_{\mathrm{Re}(b_6) h_3}^{(1)} = -\mathrm{Re}(b_6)\partial_\nu \left(X^{\dagger \nu}X_\mu + X_\mu^\dagger X^\nu \right) G^\mu - h_3 G_\mu \overline{e}\gamma^\mu e$	$\partial_+ \otimes V$
$\mathcal{L}_{\mathrm{Im}(b_6) h_3}^{(1)} = -i\mathrm{Im}(b_6)\partial_\nu \left(X^{\dagger \nu}X_\mu - X_\mu^\dagger X^\nu \right) G^\mu - h_3 G_\mu \overline{e}\gamma^\mu e$	$\partial_- \otimes V$
$\mathcal{L}_{\mathrm{Re}(b_7) h_3}^{(1)} = -\mathrm{Re}(b_7)\varepsilon_{\mu\nu\rho\sigma} \left(X^{\dagger \mu}\partial^\nu X^\rho + X^\mu \partial^\nu X^{\dagger \rho} \right) G^\sigma - h_3 G_\mu \overline{e}\gamma^\mu e$	$\varepsilon \partial_+ \otimes V$
$\mathcal{L}_{\mathrm{Im}(b_7) h_4}^{(1)} = -i\mathrm{Im}(b_7)\varepsilon_{\mu\nu\rho\sigma} \left(X^{\dagger \mu}\partial^\nu X^\rho - X^\mu \partial^\nu X^{\dagger \rho} \right) G^\sigma - h_4 G_\mu \overline{e}\gamma^\mu \gamma^5 e$	$\varepsilon \partial_- \otimes A$

Table 7. Lagrangians for a selection of simplified models with non-standard material response functions.

defines $S_i^{90\%}$ and the number of counts in each bin is assumed to obey Poisson statistics. Here, $\mathcal{P}(k \,|\, \mathcal{S}_i^{90\%})$ is the Poisson probability of observing k events when an average of $\mathcal{S}_i^{90\%}$ is expected.

By computing exclusion limits using eq. (4.7), we assume that the observed S2 or Q events do not allow one to reject the "null hypothesis" in favour of a DM discovery. For a detailed description of possible background contributions to $\mathcal{D}_i$, we refer to the experimental works [15, 23, 24, 46]. For example, environmental backgrounds and dark current events from thermal excitations are the main contributions to $\mathcal{D}_i$ in the case of SENSEI. The exclusion limits that we obtain from eq. (4.7) are conservative, as they do not rely on any background subtraction.

4.2 Constraints

We are now ready to set constraints on the models of section 2 from the null result of XENON10, XENON1T, EDELWEISS and SENSEI. While we have so far computed the DM response functions one would obtain when *all* coupling constants in a given Lagrangian from section 2 are different from zero (eqs. (3.41), (3.45), (3.46), (3.47), (3.48) and (3.49)), here we restrict ourselves to a subset of "simplified models" each characterised by four parameters, namely: the DM and mediator mass, a coupling constant for the DM-DM-mediator vertex, and a coupling constant for the electron-electron-mediator interaction vertex. This choice will simplify the discussion while still allowing us to highlight the importance of the non-standard response functions, $\overline{\mathcal{W}}_l(q, \Delta E)$, $l \neq 1$, in the non-relativistic modelling of DM-electron scattering in materials.

Specifically, we focus on the simplified models defined in table 7. The corresponding Lagrangians follow by integration by parts from the Lagrangians in section 2 when only *one pair* of coupling constants at the time is assumed to be different from zero. We focus on these eight simplified models as they generate at least one non-standard DM response function
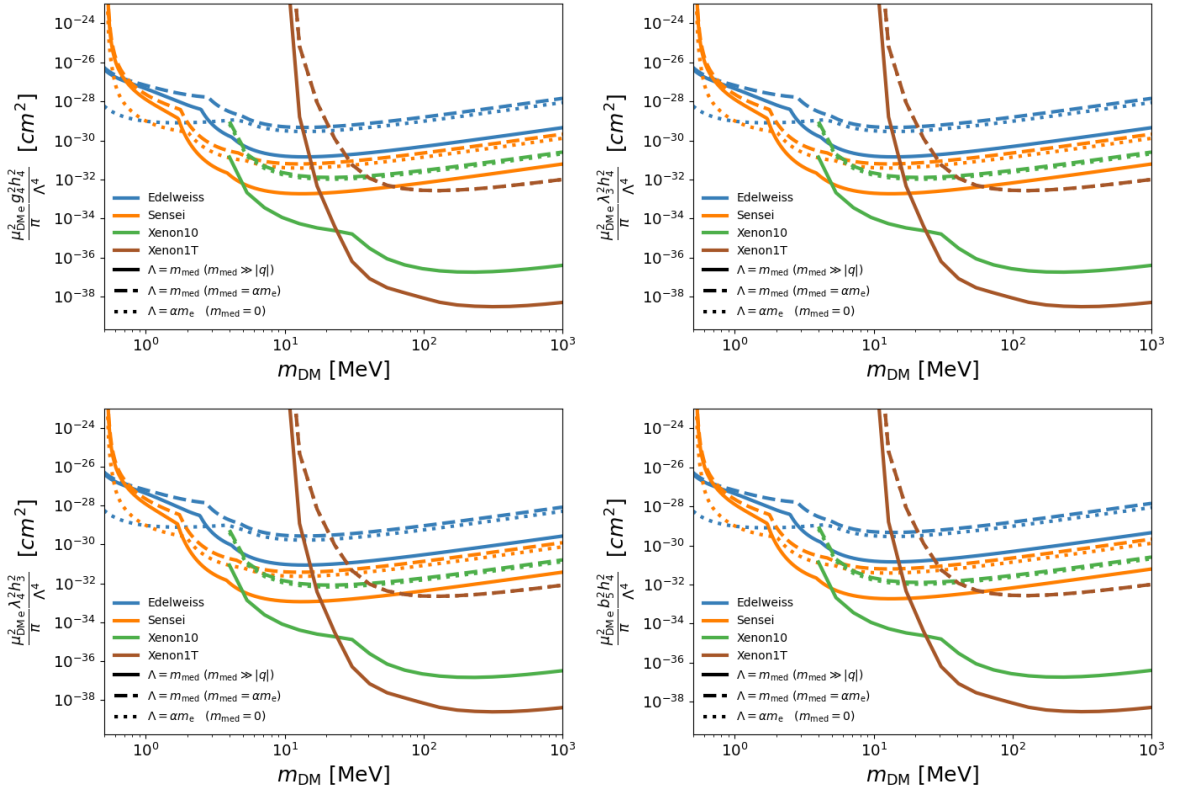
Figure 4. 90% C.L. exclusion limits on the reference cross section $\sigma_{\rm ref}$ for the simplified models with couplings constants g_4 and h_4 (top left panel), λ_3 and h_4 (top right panel), λ_4 and h_3 (bottom left panel) and b_5 and h_4 (bottom right panel). See table 7 for the corresponding Lorentz structures. Solid, dotted and dashed lines refer to long-range, "intermediate-range" with $m_{\rm med} = \alpha m_e$ and long-range interactions, while blue, orange, green and maroon lines are associated with the EDELWEISS, SENSEI, XENON10 and XENON1T experiments, respectively.

and, therefore, can only be investigated within the response function formalism we developed in [1, 2].

The Lorentz structure of the Lagrangians in table 7 is variegated. For example, $\mathcal{L}^{(0)}_{g_4 h_4}$ is characterised by a derivative coupling between scalar DM and a vector mediator, and an axial coupling between the vector mediator and the electron. Symbolically, we denote this Lorentz structure by $\partial_- \otimes A$, where the minus sign in ∂_- refers to the minus sign in parenthesis in the first term of $\mathcal{L}^{(0)}_{g_4 h_4}$. Analogously, $\mathcal{L}^{(1)}_{{\rm Re}(b_7) h_3}$ is characterised by a derivative coupling between vector DM and a vector mediator, and a vector coupling between the mediator and the electron. We denote this Lorentz structure by $\varepsilon \partial_+ \otimes V$ to emphasise that the derivative coupling in question includes a Levi-Civita tensor. By adopting the notation outlined in these examples, table 7 shows the relation between our simplified models and the underlying Lorentz structures.

For the models in table 7, we calculate 90% C.L. exclusion limits on the reference cross section,

$$\sigma_{\rm ref} = \frac{\mu^2_{\rm DMe}}{\pi} \frac{\mathcal{P}_1^2 \mathcal{P}_2^2}{\Lambda^4} , \tag{4.8}$$
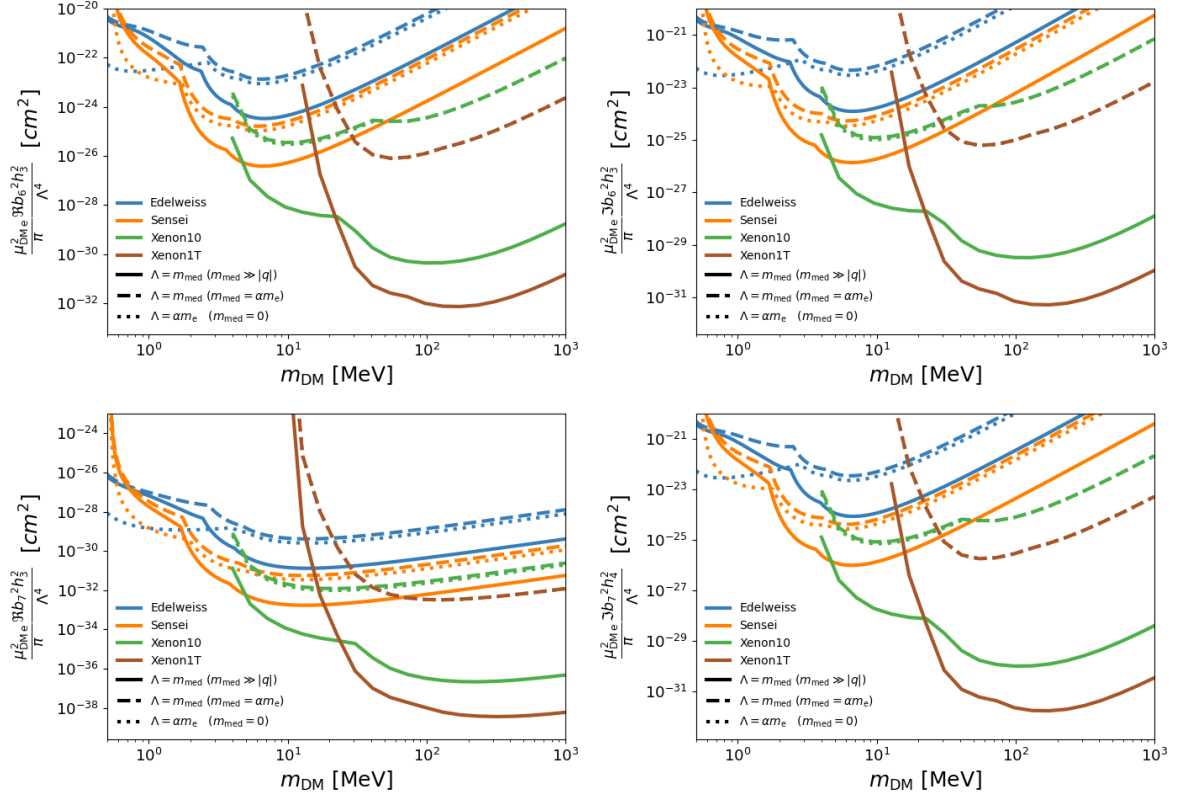
Figure 5. Same as figure 4, for the simplified models with couplings constants $\mathrm{Re}(b_6)$ and h_3 (top left), $\mathrm{Im}(b_6)$ and h_3 (top right), $\mathrm{Re}(b_7)$ and h_3 (bottom left) and $\mathrm{Im}(b_7)$ and h_4 (bottom right).

from the null result reported by the XENON10 [46], XENON1T [15], EDELWEISS [23] and SENSEI [24] collaborations. In eq. (4.8), μ_{DMe} is the DM-electron reduced mass, $\mathcal{P}_1$ and $\mathcal{P}_2$ are the coupling constants that define the given simplified model, while Λ is a reference mass scale which depends on the assumed value for the mediator mass, m_{med}. For the simplified models in table 7, we consider three cases for the mediator mass, each associated with a specific choice for Λ: 1) $m_{\mathrm{med}} \gg |\boldsymbol{q}|$, with $\Lambda = m_{\mathrm{med}}$, 2) $m_{\mathrm{med}} = \alpha m_e$, with $\Lambda = m_{\mathrm{med}}$, and, finally, 3) $m_{\mathrm{med}} = 0$, with $\Lambda = \alpha m_e$. The first (last) case corresponds to short-range (long-range) interactions, while the second one corresponds to m_{med} values that are comparable with a "reference" momentum transfer, which we set to $q_{\mathrm{ref}} = \alpha m_e$, where α is the fine structure constant.

Figure 4 shows the 90% C.L. exclusion limits on the reference cross section σ_{ref} that we obtain for the simplified models defined by the couplings constants g_4 and h_4 (top left panel), λ_3 and h_4 (top right panel), λ_4 and h_3 (bottom left panel) and b_5 and h_4 (bottom right panel). In all panels, exclusion limits are presented as a function of the DM particle mass, as well as for different mediator masses and experiments. More specifically, the solid, dotted and dashed lines in the figure refer to long-range, "intermediate-range" with $m_{\mathrm{med}} = \alpha m_e$ and long-range interactions, while blue, orange, green and maroon lines are associated with the EDELWEISS, SENSEI, XENON10 and XENON1T experiments, respectively, as indicated in the legends.

There are no appreciable differences in the exclusion limits presented in the four panels of figure 4 because the underlying simplified models either generate the operator $\mathcal{O}_7$ only in the non-relativistic limit, or linear combinations of the interaction operators $\mathcal{O}_7$ and $\mathcal{O}_8$,
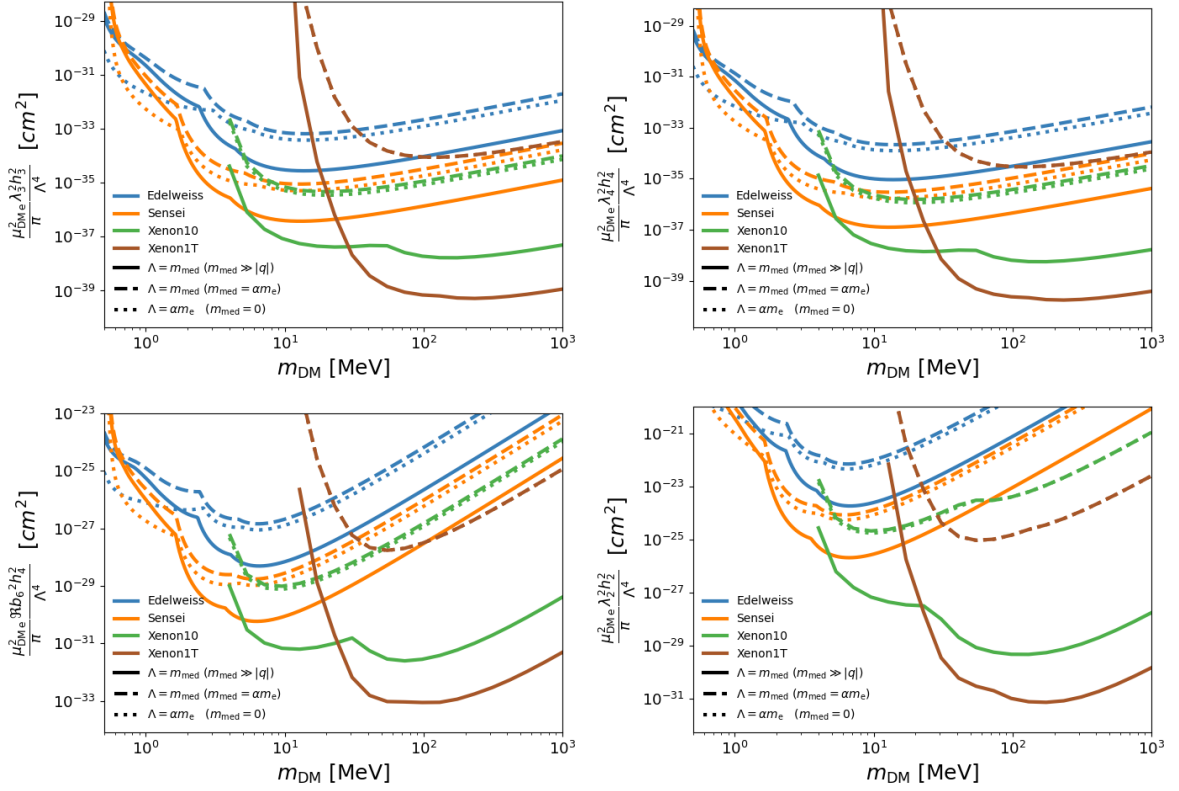
Figure 6. Same as figure 4, for the simplified models defined by the couplings constants λ_3 and h_3 (top left), λ_4 and h_4 (top right), $\text{Re}(b_6)$ and h_4 (bottom left) and λ_2 and h_2 (bottom right).

and $\mathcal{O}_7$ and $\mathcal{O}_9$. However, the operator $\mathcal{O}_7$ alone generates three non-standard material response functions.

As expected from figure 1 and figure 2, and from the fact that xenon ionisation energies are larger than germanium and silicon band gaps by an order 10 factor, for m_{DM} below about $5\,\text{MeV}$ crystal detectors such as EDELWEISS and SENSEI place stronger constraints on the cross section σ_{ref} than the xenon detectors XENON10 and XENON1T in all panels of figure 4. In contrast, XENON10 and XENON1T set stronger bounds on σ_{ref} for values of the DM particle mass that are larger than about $5\,\text{MeV}$ because of their larger experimental exposure.

In the case of XENON10 and XENON1T, exclusion limits for short-range interactions are always stronger than for long-range interactions, except near mass threshold (i.e. for m_{DM} close to the smallest testable DM mass), where they tend to overlap. Furthermore, exclusion limits for short-range and intermediate-range interactions essentially coincide. Both results are a consequence of the differential ionisation rate being proportional to σ_{ref}, $\sigma_{\text{ref}}(1+|\boldsymbol{q}|/q_{\text{ref}})^{-4}$ and $\sigma_{\text{ref}}q_{\text{ref}}^4/|\boldsymbol{q}|^4$, for long-, intermediate- and short-range interactions, and $|\boldsymbol{q}|^4/q_{\text{ref}}^4$ being typically larger than one for DM particle masses in the range probed by XENON10 and XENON1T.

In the case of EDELWEISS and SENSEI, the exclusion limits that we find in figure 4 for m_{DM} larger than about $2\,\text{MeV}$ and for different mediator masses exhibit the same hierarchy described above for XENON10 and XENON1T, the only difference being a non negligible separation between the exclusion limits obtained for short-range and intermediate-range interactions. In contrast, for DM particle masses below about $2\,\text{MeV}$, long-range interactions are associated with significantly stronger exclusion limits than short- or intermediate-range

interactions. This result can be explained by recalling the aforementioned scaling with $|\boldsymbol{q}|/q_{\rm ref}$ of the differential ionisation or excitation rate, and by noticing that for crystal detectors $|\boldsymbol{q}|/q_{\rm ref}$ is smaller than one for sufficiently small DM particle masses, as one can infer from figures 1 and 2.

Figure 5 shows the 90% C.L. exclusion limits on the reference cross section $\sigma_{\rm ref}$ that we find for the simplified models with couplings constants $\mathrm{Re}(b_6)$ and h_3 (top left panel), $\mathrm{Im}(b_6)$ and h_3 (top right panel), $\mathrm{Re}(b_7)$ and h_3 (bottom left panel) and $\mathrm{Im}(b_7)$ and h_4 (bottom right panel). The exclusion limits in figure 5 exhibit the same hierarchies and patterns discussed in details for figure 4. Importantly, none of the simplified models underlying figures 4 and 5 could have been investigated accurately without having first computed the material response functions $\overline{\mathcal{W}}_2(q, \Delta E)$ and $\overline{\mathcal{W}}_3(q, \Delta E)$ for atoms and crystals. Furthermore, we find that for vector DM models with a vector mediator also the material response function $\overline{\mathcal{W}}_4(q, \Delta E)$ is crucial.

We conclude this analysis by validating our results through a comparison with the exclusion limits associated with models that generate the material response function $\overline{\mathcal{W}}_1(q, \Delta E)$ only. Figure 6 shows our 90% C.L. exclusion limits on the reference cross section $\sigma_{\rm ref}$ for the simplified models that are identified by the couplings constants λ_3 and h_3 (top left panel), λ_4 and h_4 (top right panel), $\mathrm{Re}(b_6)$ and h_4 (bottom left panel) and λ_2 and h_2 (bottom right panel). The top panels in this figure correspond to the familiar spin-independent and spin-dependent interactions, arising from the $\mathcal{O}_1$ and $\mathcal{O}_4$ operators, respectively. The associated exclusion limits presented here agree with previous results in the literature, see e.g. [1, 2]. Notice that the (λ_3, h_3) case coincides with a dark photon model with Dirac DM. The bottom panels correspond to models that generate the $\overline{\mathcal{W}}_1(q, \Delta E)$ material response function only, but with a DM response function scaling with $|\boldsymbol{q}|^2$ (left panel) and $|\boldsymbol{q}|^4$ (right panel), respectively.

5   Summary and conclusion

A still open question in the field of sub-GeV DM direct detection is whether experimental results can be interpreted within a theoretical framework where the response of detector materials is described in terms of a single ionisation or crystal form factors only, as in the case of the dark photon model. In this work, we have addressed this question by computing the rate of electronic transitions induced by DM-electron scattering in isolated xenon atoms, as well as in silicon and germanium crystals, for a variety of models where the DM particle can have spin 0, spin 1/2 or spin 1, while the particle that mediates the DM-electron interaction can have either spin 0 or spin 1. We have found several examples for which an accurate description of the non-relativistic scattering of DM particles by the electrons bound in detector materials requires material response functions that go beyond the standard ionisation and crystal form factors. For simplicity, we have illustrated this conclusion by restricting ourselves to the case of "simplified model", where just two coupling constants at the time are different from zero. However, the fact that non-standard material response functions can arise in "minimal extensions" of the dark photon model is a general conclusion of our study, which does not rely on this restriction. This result corroborates our previous findings [1, 2], and shows the importance of a response function formalism in the interpretation of future DM direct detection data.

For the eight models that generate a non-standard material response, we have calculated 90% C.L. exclusion limits on the reference cross section for DM-electron electron scattering, eq. (4.8), from the null result reported by the XENON10 [46], XENON1T [15],

EDELWEISS [23] and SENSEI [24] experiments. We have performed this calculation as a function of the DM particle mass and for different values of the mediator mass. We have not only considered small and large mediator masses, corresponding to contact and long range interactions, but also scenarios in which the mediator mass is comparable with the momentum transfer in the scattering. Importantly, none of these exclusion limits could have accurately been extracted from data without having first computed the non-standard material response functions of section 3.

A byproduct of our analysis is eq. (3.28) which, expanding on our previous work [1, 2], has enabled us to express the response of xenon and crystal detectors to an external DM probe in the same, compact form (which was not the case in [1, 2]). An interesting aspect of this equation is that it allows for a simple comparison of the performance of different materials in the context of sub-GeV DM direct detection. We have applied this result to compare the response of xenon, silicon and germanium detectors finding that these materials perform best in complementary regions of the plane spanned by the momentum transfer and the deposited energy.

To conclude, we give a positive answer to the question of whether new material response functions beyond the standard crystal and ionisation form factors are needed for the interpretation of present and future direct detection experiments searching for DM-induced electronic transitions.

Acknowledgments

A Squared transition amplitudes

Here, we provide the details underling the derivation of eqs. (3.46), (3.47), (3.48) and (3.49). These four equations correspond to the DM response functions for, respectively, fermionic dark matter with a scalar mediator, fermionic dark matter with a vector mediator, vector dark matter with a scalar mediator and, finally, vector dark matter with a vector mediator.

A.1 Fermionic dark matter with a scalar mediator

The free amplitude for DM-electron scattering in the case of spin-1/2 DM with a scalar mediator is

$$i\mathcal{M} = \overline{u}_\chi^{s'}(p')i(\lambda_1 + i\lambda_2\gamma^5)u_\chi^s(p)\frac{i}{(p-p')^2 - m_\phi^2}\overline{u}_e^{r'}(k')i(h_1 + ih_2\gamma^5)u_e^r(k)\,, \qquad (A.1)$$

where u_e^r and u_χ^s are electron and DM free spinors, while k and k' (p and p') are the initial and final electron (DM) four-momenta. By using the spinor bilinear expansions in appendix B, we

find that in the non-relativistic limit the amplitude $i\mathcal{M}$ in eq. (A.1) can be written as follows

$$i\mathcal{M} \simeq i4m_\chi m_e \left(\frac{\lambda_1 h_1}{|\boldsymbol{q}|^2 + m_\phi^2} \langle \mathcal{O}_1 \rangle + \frac{\lambda_2 h_2}{|\boldsymbol{q}|^2 + m_\phi^2} \frac{m_e}{m_\chi} \langle \mathcal{O}_6 \rangle - \frac{\lambda_1 h_2}{|\boldsymbol{q}|^2 + m_\phi^2} \langle \mathcal{O}_{10} \rangle \right. $$
$$\left. + \frac{\lambda_2 h_1}{|\boldsymbol{q}|^2 + m_\phi^2} \frac{m_e}{m_\chi} \langle \mathcal{O}_{11} \rangle \right) . \tag{A.2}$$

The operators appearing in angle brackets in this expression are listed in table 1. From eq. (A.2), we find

$$\overline{|\mathcal{M}|^2} |f_{1\to 2}|^2 = \left(c_1^2 + \frac{1}{16} c_6^2 \frac{|\boldsymbol{q}|^4}{m_e^4} + \frac{1}{4} c_{10}^2 \frac{|\boldsymbol{q}|^2}{m_e^2} + \frac{1}{4} c_{11}^2 \frac{|\boldsymbol{q}|^2}{m_e^2} \right) |f_{1\to 2}|^2$$

$$2m_e \mathrm{Re} \left\{ \overline{\mathcal{M} f_{1\to 2} [\nabla_\ell \mathcal{M}^*] \cdot \boldsymbol{f}_{1\to 2}^*} \right\} = 0$$

$$m_e^2 \overline{|\nabla_\ell \mathcal{M}(\boldsymbol{q}, \boldsymbol{v}_{\mathrm{el}}^\perp)] \cdot \boldsymbol{f}_{1\to 2}(\boldsymbol{q})|^2} = 0 \,, \tag{A.3}$$

which implies eq. (3.46), once the azimuthal average in eq. (3.33) is computed by using eq. (3.35). We give the relation between the non-relativistic coupling constants in the equations above, i.e. c_1, c_6, c_{10} and c_{11}, and the particle masses and coupling constants in eq. (A.2) in table 3. Here and below, we implicitly assume that $\mathcal{M}$ bilinears are evaluated at $\ell = 0$ and $\cos\theta = \xi$.

A.2 Fermionic dark matter with a vector mediator

In the case of spin-1/2 DM with a vector mediator, the free amplitude for DM-electron scattering is

$$i\mathcal{M} = \left[\overline{u}^{s'}(p')_\chi i(\lambda_3 \gamma_\mu + \lambda_4 \gamma_\mu \gamma^5) u_\chi^s(p) \right] \frac{-ig^{\mu\nu}}{(p-p')^2 - m_G^2} \left[\overline{u}_e^{r'}(k') i(h_3 \gamma_\nu + h_4 \gamma_\nu \gamma^5) u_e^r(k) \right] , \tag{A.4}$$

which, reduces to

$$i\mathcal{M} \simeq i4m_\chi m_e \left[-\frac{\lambda_3 h_3}{|\boldsymbol{q}|^2 + m_G^2} \langle \hat{\mathcal{O}}_1 \rangle + \frac{4\lambda_4 h_4}{|\boldsymbol{q}|^2 + m_G^2} \langle \hat{\mathcal{O}}_4 \rangle + \frac{2\lambda_3 h_4}{|\boldsymbol{q}|^2 + m_G^2} \langle \hat{\mathcal{O}}_7 \rangle - \frac{2\lambda_4 h_3}{|\boldsymbol{q}|^2 + m_G^2} \langle \hat{\mathcal{O}}_8 \rangle \right.$$

$$\left. + \left(\frac{2\lambda_3 h_4}{|\boldsymbol{q}|^2 + m_G^2} \frac{m_e}{m_\chi} + \frac{2\lambda_4 h_3}{|\boldsymbol{q}|^2 + m_G^2} \right) \langle \hat{\mathcal{O}}_9 \rangle \right] , \tag{A.5}$$

in the non-relativistic limit. We give explicit expressions for the operators and coupling constants in this equation in table 1 and table 3, respectively. Finally, by applying eq. (A.5), we obtain

$$\overline{|\mathcal{M}|^2} |f_{1\to 2}|^2 = \left(c_1^2 + \frac{3}{16} c_4^2 + \frac{1}{4} c_7^2 |\boldsymbol{v}_{\mathrm{el}}^\perp|^2 + \frac{1}{4} c_8^2 |\boldsymbol{v}_{\mathrm{el}}^\perp|^2 + \frac{1}{8} c_9^2 \frac{|\boldsymbol{q}|^2}{m_e^2} \right) |f_{1\to 2}|^2$$

$$2m_e \mathrm{Re} \left\{ \overline{\mathcal{M} f_{1\to 2} [\nabla_\ell \mathcal{M}^*] \cdot \boldsymbol{f}_{1\to 2}^*} \right\} = -\left(\frac{1}{2} c_7^2 + \frac{1}{2} c_8^2 \right) \boldsymbol{v}_{\mathrm{el}}^\perp \cdot \mathrm{Re} \left(\boldsymbol{f}_{1\to 2}^* f_{1\to 2} \right)$$

$$m_e^2 \overline{|\nabla_\ell \mathcal{M}(\boldsymbol{q}, \boldsymbol{v}_{\mathrm{el}}^\perp)] \cdot \boldsymbol{f}_{1\to 2}(\boldsymbol{q})|^2} = \left(\frac{1}{4} c_7^2 + \frac{1}{4} c_8^2 \right) |\boldsymbol{f}_{1\to 2}|^2 \,. \tag{A.6}$$

By taking the azimuthal average of the equations above, we obtain the DM response functions in eq. (3.47).

A.3 Vector dark matter with a scalar mediator

The free amplitude for DM-electron scattering in the case of spin-1 DM with a scalar mediator is

$$i\mathcal{M} = \left[i(b_1 m_X g^{\mu\nu})\varepsilon_\mu^{*s'}(p')\varepsilon_\nu^s(p)\right] \frac{i}{(p-p')^2 - m_\phi^2} \left[\overline{u}_e^{r'}(k')i(h_1 + ih_2\gamma^5)u_e^r(k)\right], \qquad \text{(A.7)}$$

and, in the non-relativistic limit,

$$i\mathcal{M} \simeq i4m_X m_e \left(\frac{1}{2}\frac{b_1 h_1}{|\mathbf{q}|^2 + m_\phi^2}\langle\hat{\mathcal{O}}_1\rangle - \frac{1}{2}\frac{b_1 h_2}{|\mathbf{q}|^2 + m_\phi^2}\langle\hat{\mathcal{O}}_{10}\rangle\right), \qquad \text{(A.8)}$$

from which

$$\overline{|\mathcal{M}|^2}|f_{1\to2}|^2 = \left(c_1^2 + \frac{1}{4}c_{10}^2\frac{|\mathbf{q}|^2}{m_e^2}\right)|f_{1\to2}|^2$$

$$2m_e\text{Re}\left\{\overline{\mathcal{M}f_{1\to2}[\nabla_\ell\mathcal{M}^*]\cdot\mathbf{f}_{1\to2}^*}\right\} = 0$$

$$m_e^2\overline{|\nabla_\ell\mathcal{M}(\mathbf{q},\mathbf{v}_{\text{el}}^\perp)]\cdot\mathbf{f}_{1\to2}(\mathbf{q})|^2} = 0. \qquad \text{(A.9)}$$

The operators $\mathcal{O}_1$ and $\mathcal{O}_{10}$ are defined in table 1, whereas an explicit relation between c_1 and c_{10} and the masses and coupling constants in eq. (A.8) can be found in table 4. As a result, eq. (3.48) follows from eq. (A.9) by a straightforward application of the definition (3.33) and eq. (3.35).

A.4 Vector dark matter with a vector mediator

Finally, in the case of spin-1 DM with a vector mediator the free amplitude for DM-electron scattering is

$$\begin{aligned}
i\mathcal{M} = \Bigg[&- ib_5\left(p'^\mu + p^\mu\right)\varepsilon^{s'\nu*}(p')\varepsilon_\nu^s(p) \\
&+ \text{Re}(b_6)\left(p'_\nu - p_\nu\right)\left(\varepsilon^{s'\nu*}(p')\varepsilon^{s\mu}(p) + \varepsilon^{s'\mu*}(p')\varepsilon^{s\nu}(p)\right) \\
&+ i\text{Im}(b_6)\left(p'_\nu - p_\nu\right)\left(\varepsilon^{s'\nu*}(p')\varepsilon^{s\mu}(p) - \varepsilon^{s'\mu*}(p')\varepsilon^{s\nu}(p)\right) \\
&- \text{Re}(b_7)\varepsilon_{\alpha\nu\rho\sigma}\left(p'^\nu + p^\nu\right)\varepsilon^{s'\alpha*}(p')\varepsilon^{s\rho}(p)\eta^{\sigma\mu} \\
&+ i\text{Im}(b_7)\varepsilon_{\alpha\nu\rho\sigma}\left(p'^\nu - p^\nu\right)\varepsilon^{s'\alpha*}(p')\varepsilon^{s\rho}(p)\eta^{\sigma\mu}\Bigg] \\
&\times \left[\frac{-1}{(p-p')^2 - m_G^2}\right]\overline{u}_e^{r'}(k')\gamma_\mu(h_3 + h_4\gamma_5)u_e^r(k).
\end{aligned} \qquad \text{(A.10)}$$

By using the results listed in appendix B, we find that in the non-relativistic limit eq. (A.10) reduces to

$$
\begin{aligned}
i\mathcal{M} \simeq i4m_X m_e \Bigg[& -\frac{b_5 h_3}{|\boldsymbol{q}|^2 + m_G^2}\langle\hat{\mathcal{O}}_1\rangle + \left(\frac{\mathrm{Im}(b_6)h_3}{|\boldsymbol{q}|^2 + m_G^2}\frac{m_e}{2m_X}\frac{|\boldsymbol{q}|^2}{m_e^2} - \frac{2\mathrm{Re}(b_7)h_4}{|\boldsymbol{q}|^2 + m_G^2}\right)\langle\hat{\mathcal{O}}_4\rangle \\
& + \frac{\mathrm{Im}(b_6)h_3}{|\boldsymbol{q}|^2 + m_G^2}\frac{m_e}{2m_X}\langle\hat{\mathcal{O}}_5\rangle - \frac{\mathrm{Im}(b_6)h_3}{|\boldsymbol{q}|^2 + m_G^2}\frac{m_e}{2m_X}\langle\hat{\mathcal{O}}_6\rangle + \frac{2b_5 h_4}{|\boldsymbol{q}|^2 + m_G^2}\langle\hat{\mathcal{O}}_7\rangle \\
& + \frac{\mathrm{Re}(b_7)h_3}{|\boldsymbol{q}|^2 + m_G^2}\langle\hat{\mathcal{O}}_8\rangle + \left(\frac{\mathrm{Im}(b_6)h_4}{|\boldsymbol{q}|^2 + m_G^2}\frac{m_e}{m_X} - \frac{\mathrm{Re}(b_7)h_3}{|\boldsymbol{q}|^2 + m_G^2}\right)\langle\hat{\mathcal{O}}_9\rangle \\
& + \frac{1}{2}\frac{\mathrm{Im}(b_7)h_3}{|\boldsymbol{q}|^2 + m_G^2}\frac{m_e}{m_X}\langle\hat{\mathcal{O}}_{11}\rangle - \frac{\mathrm{Im}(b_7)h_4}{|\boldsymbol{q}|^2 + m_G^2}\frac{m_e}{m_X}\langle\hat{\mathcal{O}}_{14}\rangle \\
& - \frac{\mathrm{Re}(b_6)h_3}{|\boldsymbol{q}|^2 + m_G^2}\frac{m_e}{m_X}\langle\hat{\mathcal{O}}_{17}\rangle + \frac{2\mathrm{Re}(b_6)h_4}{|\boldsymbol{q}|^2 + m_G^2}\frac{m_e}{m_X}\langle\hat{\mathcal{O}}_{18}\rangle + \frac{\mathrm{Im}(b_6)h_3}{|\boldsymbol{q}|^2 + m_G^2}\frac{m_e^2}{2m_X^2}\langle\hat{\mathcal{O}}_{19}\rangle \\
& - \left(\frac{\mathrm{Re}(b_6)h_3}{|\boldsymbol{q}|^2 + m_G^2}\frac{m_e}{m_X} + \frac{\mathrm{Im}(b_7)h_4}{|\boldsymbol{q}|^2 + m_G^2}\frac{m_e^2}{m_X^2}\right)\langle\hat{\mathcal{O}}_{20}\rangle \Bigg].
\end{aligned} \tag{A.11}
$$

As above, we define the operators in eq. (A.11) in table 1. From eq. (A.11), we obtain the expressions

$$
\begin{aligned}
\overline{|\mathcal{M}|^2}|f_{1\to 2}|^2 = \Bigg(& c_1^2 + \frac{1}{2}c_4^2 + \frac{2}{3}c_5^2 \Big|\frac{\boldsymbol{q}}{m_e}\times\boldsymbol{v}_{\mathrm{el}}^\perp\Big|^2 + \frac{1}{6}c_6^2\frac{|\boldsymbol{q}|^4}{m_e^4} + \frac{1}{4}c_7^2|\boldsymbol{v}_{\mathrm{el}}^\perp|^2 \\
& + \frac{2}{3}c_8^2|\boldsymbol{v}_{\mathrm{el}}^\perp|^2 + \frac{1}{3}c_9^2\frac{|\boldsymbol{q}|^2}{m_e^2} + \frac{2}{3}c_{11}^2\frac{|\boldsymbol{q}|^2}{m_e^2} + \frac{1}{6}c_{14}^2|\boldsymbol{v}_{\mathrm{el}}^\perp|^2\frac{|\boldsymbol{q}|^2}{m_e^2} \\
& + \frac{1}{6}c_{17}^2\left(\Big|\frac{\boldsymbol{q}}{m_e}\cdot\boldsymbol{v}_{\mathrm{el}}^\perp\Big|^2 + \frac{|\boldsymbol{q}|^2}{m_e^2}|\boldsymbol{v}_{\mathrm{el}}^\perp|^2\right) + \frac{1}{6}c_{18}^2\frac{|\boldsymbol{q}|^2}{m_e^2} \\
& + \frac{1}{3}c_{19}^2\frac{|\boldsymbol{q}|^4}{m_e^4} + \frac{1}{12}c_{20}^2\frac{|\boldsymbol{q}|^4}{m_e^4} + \frac{1}{3}c_4 c_6\frac{|\boldsymbol{q}|^2}{m_e^2} + \frac{2}{3}c_1 c_{19}\frac{|\boldsymbol{q}|^2}{m_e^2} \Bigg)|f_{1\to 2}|^2 \\
2m_e\mathrm{Re}\left\{\overline{\mathcal{M}f_{1\to 2}[\nabla_\ell\mathcal{M}^*]\cdot\boldsymbol{f}_{1\to 2}^*}\right\} = & \left[\frac{\boldsymbol{q}}{m_e}\cdot\boldsymbol{v}_{\mathrm{el}}^\perp\left(\frac{4}{3}c_5^2 - \frac{1}{3}c_{17}^2\right)\right]\frac{\boldsymbol{q}}{m_e}\cdot\mathrm{Re}\left(\boldsymbol{f}_{1\to 2}^* f_{1\to 2}\right) \\
& - \left[\frac{1}{2}c_7^2 + \frac{4}{3}c_8^2 + \frac{|\boldsymbol{q}|^2}{m_e^2}\left(\frac{4}{3}c_5^2 + \frac{1}{3}c_{14}^2 + \frac{1}{3}c_{17}^2\right)\right] \\
& \times\boldsymbol{v}_{\mathrm{el}}^\perp\cdot\mathrm{Re}\left(\boldsymbol{f}_{1\to 2}^* f_{1\to 2}\right) \\
m_e^2\overline{|[\nabla_\ell\mathcal{M}(\boldsymbol{q},\boldsymbol{v}_{\mathrm{el}}^\perp)]\cdot\boldsymbol{f}_{1\to 2}(\boldsymbol{q})|^2} = & \left[\frac{1}{4}c_7^2 + \frac{2}{3}c_8^2 + \frac{|\boldsymbol{q}|^2}{m_e^2}\left(\frac{2}{3}c_5^2 + \frac{1}{6}c_{14}^2 + \frac{1}{6}c_{17}^2\right)\right]|\boldsymbol{f}_{1\to 2}|^2 \\
& + \left(-\frac{2}{3}c_5^2 + \frac{1}{6}c_{17}^2\right)\left|\frac{\boldsymbol{q}}{m_e}\cdot\boldsymbol{f}_{1\to 2}\right|^2,
\end{aligned} \tag{A.12}
$$

from which eq. (3.49) follows by computing an azimuthal average, as shown explicitly in eq. (3.35). As in the previous examples, the coupling constants in eq. (A.12) are defined in table 4.

B Useful identities

Below, we list expressions that we use in the non-relativistic reduction of free scattering amplitudes, and in the calculation of the squared modulus of the transition amplitude for the models in section 2. We start from the non-relativistic reduction of free spinors and spinor bilinears,

$$u_\chi^r(p) \simeq \frac{1}{\sqrt{4m_\chi}} \begin{pmatrix} (2m_\chi - \boldsymbol{p} \cdot \boldsymbol{\sigma})\xi^r \\ (2m_\chi + \boldsymbol{p} \cdot \boldsymbol{\sigma})\xi^r \end{pmatrix},$$

and

$$\overline{u}_\chi^{s'}(p')u_\chi^s(p) \simeq 2m_\chi\, \xi^{\dagger s'}\xi^s \tag{B.1}$$

$$\overline{u}_\chi^{s'}(p')i\gamma^5 u_\chi^s(p) \simeq 2i\boldsymbol{q} \cdot \boldsymbol{s}^{s's} \tag{B.2}$$

$$\overline{u}_\chi^{s'}(p')\gamma^\mu u_\chi^s(p) \simeq \begin{pmatrix} 2m_\chi\, \xi^{\dagger s'}\xi^s \\ \boldsymbol{P}\, \xi^{\dagger s'}\xi^s + 2i\boldsymbol{q} \times \boldsymbol{s}^{s's} \end{pmatrix} \tag{B.3}$$

$$\overline{u}_\chi^{s'}(p')\gamma^\mu\gamma^5 u_\chi^s(p) \simeq \begin{pmatrix} 2\boldsymbol{P} \cdot \boldsymbol{s}^{s's} \\ 4m_\chi\, \boldsymbol{s}^{s's} \end{pmatrix} \tag{B.4}$$

$$\overline{u}_\chi^{s'}(p')\sigma^{\mu\nu} u_\chi^s(p) \simeq \begin{pmatrix} 0 & i\boldsymbol{q}\, \xi^{\dagger s'}\xi^s - 2\boldsymbol{P} \times \boldsymbol{s}^{s's} \\ -i\boldsymbol{q}\, \xi^{\dagger s'}\xi^s + 2\boldsymbol{P} \times \boldsymbol{s}^{s's} & 4m_\chi\, \varepsilon_{ijk}\, s^{s'sk} \end{pmatrix}, \tag{B.5}$$

respectively, which apply to the case of fermionic DM. Here, $\boldsymbol{s}^{s's} \equiv \xi^{\dagger s'}\boldsymbol{S}_{\mathrm{DM}}\xi^s$, $\boldsymbol{P} = \boldsymbol{p} + \boldsymbol{p}'$, $\boldsymbol{q} = \boldsymbol{p} - \boldsymbol{p}'$, ξ^s, $s = 1, 2$ and $\xi^{\dagger s'}$, $s' = 1, 2$ are two component spinors, while $\boldsymbol{\sigma} = (\sigma_1, \sigma_2, \sigma_3)$ is a vector the component of which are the three Pauli matrices. Similar expressions apply to the free electron spinor u_e^r. In the non-relativistic reduction of scattering amplitudes, we also use the polarisation vectors of massive vector DM or spin-1 mediator particles. They can be expanded as

$$\varepsilon_\mu^{s\mu}(\boldsymbol{p}) \simeq \begin{pmatrix} \frac{1}{2m_X}(\boldsymbol{P} + \boldsymbol{q}) \cdot \boldsymbol{e}_s \\ \boldsymbol{e}_s \end{pmatrix} \qquad \varepsilon^{s'\mu*}(\boldsymbol{p}') \simeq \begin{pmatrix} \frac{1}{2m_X}(\boldsymbol{P} - \boldsymbol{q}) \cdot \boldsymbol{e}'_{s'} \\ \boldsymbol{e}'_{s'} \end{pmatrix}, \tag{B.6}$$

where $s, s' = 1, 2, 3$, m_X can be either the DM or the mediator mass, $\boldsymbol{e}_3 = \boldsymbol{p}/|\boldsymbol{p}|$, $\boldsymbol{e}'_{3'} = \boldsymbol{p}'/|\boldsymbol{p}'|$, and $\boldsymbol{e}_s \cdot \boldsymbol{e}'_{s'} \simeq \delta_{ss'}$. In addition, we use the non-relativistic expansion of the momentum transfer four-vector,

$$q \equiv (E_{\boldsymbol{p}} - E_{\boldsymbol{p}'}, \boldsymbol{p} - \boldsymbol{p}') \simeq \left(\frac{\boldsymbol{P} \cdot \boldsymbol{q}}{2m_{\mathrm{DM}}}, \boldsymbol{q} \right), \tag{B.7}$$

which allows us to write the non-relativistic reduction of scattering amplitudes in terms of $\boldsymbol{q}$ and

$$\boldsymbol{v}_{\mathrm{el}}^\perp = \frac{\boldsymbol{p} + \boldsymbol{p}'}{2m_{\mathrm{DM}}} - \frac{\boldsymbol{k} + \boldsymbol{k}'}{2m_e} = \boldsymbol{v} - \frac{\boldsymbol{k}}{m_e} - \frac{\boldsymbol{q}}{2\mu_{\mathrm{DMe}}}, \tag{B.8}$$

where $\boldsymbol{k}$ ($\boldsymbol{k}'$) is the initial (final) free electron momentum, and $\boldsymbol{v}$ the DM-electron relative velocity. We conclude this appendix by listing useful spin sums for electrons or spin-1/2 DM particles,

$$\frac{1}{2}\sum_{r'r} |\boldsymbol{s}^{r'r}|^2 = \frac{3}{4} \qquad\qquad \frac{1}{2}\sum_{r'r} (\boldsymbol{s}^{r'r} \times \boldsymbol{A}) \cdot \boldsymbol{s}^{r'r} = 0 \tag{B.9}$$

$$\frac{1}{2}\sum_{r'r}(\boldsymbol{s}^{r'r}\cdot\boldsymbol{A})(\boldsymbol{s}^{r'r}\cdot\boldsymbol{B})=\frac{1}{4}\boldsymbol{A}\cdot\boldsymbol{B} \qquad\qquad \frac{1}{2}\sum_{r'r}(\boldsymbol{s}^{r'r}\cdot\boldsymbol{A})\delta^{r'r}=0 \qquad (\text{B.10})$$

$$\frac{1}{2}\sum_{r'r}(\boldsymbol{s}^{r'r}\times\boldsymbol{A})(\boldsymbol{s}^{r'r}\times\boldsymbol{B})=\frac{1}{2}\boldsymbol{A}\cdot\boldsymbol{B} \qquad\qquad \frac{1}{2}\sum_{r'r}(\boldsymbol{s}^{r'r}\times\boldsymbol{A})\delta^{r'r}=0 \qquad (\text{B.11})$$

and for spin-1 DM particles,

$$\frac{1}{3}\sum_{s's}\boldsymbol{A}\cdot\boldsymbol{s}_V^{s's}=0 \qquad (\text{B.12})$$

$$\frac{1}{3}\sum_{s's}\boldsymbol{A}\cdot\mathcal{S}^{s's}\cdot\boldsymbol{s}_V^{s's}=0 \qquad (\text{B.13})$$

$$\frac{1}{3}\sum_{s's}(\boldsymbol{A}\cdot\boldsymbol{s}_V^{s's})(\boldsymbol{B}\cdot\boldsymbol{s}_V^{s's})=\frac{2}{3}\boldsymbol{A}\cdot\boldsymbol{B} \qquad (\text{B.14})$$

$$\frac{1}{3}\sum_{s's}(\boldsymbol{A}\times\boldsymbol{s}_V^{s's})\cdot(\boldsymbol{B}\times\boldsymbol{s}_V^{s's})=\frac{4}{3}\boldsymbol{A}\cdot\boldsymbol{B} \qquad (\text{B.15})$$

$$\frac{1}{3}\sum_{s's}(\boldsymbol{A}\cdot\mathcal{S}^{s's}\cdot\boldsymbol{B})\delta^{s's}=\frac{1}{3}\boldsymbol{A}\cdot\boldsymbol{B} \qquad (\text{B.16})$$

$$\frac{1}{3}\sum_{s's}(\boldsymbol{A}\cdot\mathcal{S}^{s's}\cdot\boldsymbol{B})(\boldsymbol{s}_V^{s's}\cdot\boldsymbol{C})=0 \qquad (\text{B.17})$$

$$\frac{1}{3}\sum_{s's}(\boldsymbol{A}\cdot\mathcal{S}^{s's})\cdot(\boldsymbol{B}\cdot\mathcal{S}^{s's})=\frac{2}{3}\boldsymbol{A}\cdot\boldsymbol{B} \qquad (\text{B.18})$$

$$\frac{1}{3}\sum_{s's}|\boldsymbol{A}\cdot\mathcal{S}^{s's}\cdot\boldsymbol{B}|^2=\frac{1}{6}|\boldsymbol{A}\cdot\boldsymbol{B}|^2+\frac{1}{6}|\boldsymbol{A}|^2|\boldsymbol{B}|^2\,, \qquad (\text{B.19})$$

where $\boldsymbol{A}$ and $\boldsymbol{B}$ are arbitrary three-dimensional vectors, $r=1,2$, $r'=1,2$, $s=1,2,3$, $s'=1,2,3$, and

$$\boldsymbol{s}_V^{s's}\equiv-i\boldsymbol{e}'_{s'}\times\boldsymbol{e}_s \qquad (\text{B.20})$$

$$\mathcal{S}_{ij}^{s's}\equiv\frac{1}{2}(e_{si}e'_{s'j}+e_{sj}e'_{s'i})\,. \qquad (\text{B.21})$$

The expressions above are useful in the evaluation of the squared modulus of transition amplitudes.

C One-loop amplitudes

Below, we list the free electron amplitudes for the four diagrams in figure 1 in the non-relativistic limit.

1. *Scalar DM with a scalar mediator.* For the top left diagram in figure 1, we obtain the amplitude

$$\begin{aligned} i\mathcal{M}\simeq-i4m_Sm_e\Bigg[&\frac{g_2h_1^2}{2}\frac{m_e}{m_S}\frac{\delta_{\lceil h_2\rceil 0}}{(4\pi)^2}\int_0^1\mathrm{d}x\int_0^{1-x}\mathrm{d}y\frac{x+y+1}{\Delta}\\ &+\frac{g_2h_2^2}{2}\frac{m_e}{m_S}\frac{\delta_{\lceil h_1\rceil 0}}{(4\pi)^2}\int_0^1\mathrm{d}x\int_0^{1-x}\mathrm{d}y\frac{x+y-1}{\Delta}\Bigg]\langle\hat{\mathcal{O}}_1\rangle\,, \qquad (\text{C.1}) \end{aligned}$$

where we assume that the only coupling constants different from zero are either g_2 and h_1, or g_2 and h_1, while

$$\Delta = (x^2 + y^2)m_e^2 + (x+y)(m_M^2 - m_e^2) + xy|\boldsymbol{q}|^2 + (1 - x - y + 2xy)m_e^2, \qquad (C.2)$$

with $m_M = m_\phi$.

2. *Scalar DM with a vector mediator.* The amplitude for the top right diagram in figure 1 is equal to

$$
\begin{aligned}
i\mathcal{M} \simeq i4m_S m_e \Bigg[& g_3 h_3^2 \frac{m_e}{m_S} \frac{\delta_{\lceil h_4 \rceil 0}}{(4\pi)^2} \int_0^1 \mathrm{d}x \int_0^{1-x} \mathrm{d}y \frac{x+y-2}{\Delta} \\
& + g_3 h_4^2 \frac{m_e}{m_S} \frac{\delta_{\lceil h_3 \rceil 0}}{(4\pi)^2} \int_0^1 \mathrm{d}x \int_0^{1-x} \mathrm{d}y \frac{x+y+2}{\Delta} \Bigg] \langle \hat{\mathcal{O}}_1 \rangle
\end{aligned}
\qquad (C.3)
$$

where Δ is given in eq. (C.2) with $m_M = m_G$. In this latter equation, we assume that the coupling constants g_3 and h_3, or g_3 and h_4, are the only ones being different from zero in the Lagrangian.

3. *Vector DM with a scalar mediator.* For the bottom left diagram in figure 1, we find the amplitude

$$
\begin{aligned}
i\mathcal{M} \simeq -i4m_X m_e \Bigg[& \frac{b_2 h_1^2}{2} \frac{m_e}{m_X} \frac{\delta_{\lceil h_2 \rceil 0}}{(4\pi)^2} \int_0^1 \mathrm{d}x \int_0^{1-x} \mathrm{d}y \frac{x+y+1}{\Delta} \\
& + \frac{b_2 h_2^2}{2} \frac{m_e}{m_X} \frac{\delta_{\lceil h_1 \rceil 0}}{(4\pi)^2} \int_0^1 \mathrm{d}x \int_0^{1-x} \mathrm{d}y \frac{x+y-1}{\Delta} \Bigg] \langle \hat{\mathcal{O}}_1 \rangle,
\end{aligned}
\qquad (C.4)
$$

where $m_M = m_\phi$ in Δ, and either b_2 and h_1, or b_2 and h_1 are the only non-zero coupling constants.

4. *Vector DM with a vector mediator.* Finally, the amplitude for the bottom right diagram in figure 1 is

$$
\begin{aligned}
i\mathcal{M} \equiv i4m_X m_e \Bigg[& b_3 h_3^2 \frac{m_e}{m_X} \frac{\delta_{\lceil h_4 \rceil 0}\delta_{\lceil b_4 \rceil 0}}{(4\pi)^2} \int_0^1 \mathrm{d}x \int_0^{1-x} \mathrm{d}y \frac{x+y-2}{\Delta} \\
& + b_3 h_4^2 \frac{m_e}{m_X} \frac{\delta_{\lceil h_3 \rceil 0}\delta_{\lceil b_4 \rceil 0}}{(4\pi)^2} \int_0^1 \mathrm{d}x \int_0^{1-x} \mathrm{d}y \frac{x+y+2}{\Delta} \\
& + \frac{b_4 h_3^2}{2} \frac{m_e}{m_X} \frac{\delta_{\lceil h_4 \rceil 0}\delta_{\lceil b_3 \rceil 0}}{(4\pi)^2} \int_0^1 \mathrm{d}x \int_0^{1-x} \mathrm{d}y \frac{x+y-1}{\Delta} \\
& + \frac{b_4 h_4^2}{2} \frac{m_e}{m_X} \frac{\delta_{\lceil h_3 \rceil 0}\delta_{\lceil b_3 \rceil 0}}{(4\pi)^2} \int_0^1 \mathrm{d}x \int_0^{1-x} \mathrm{d}y \frac{x+y+1}{\Delta} \Bigg] \langle \hat{\mathcal{O}}_1 \rangle,
\end{aligned}
\qquad (C.5)
$$

where only b_3 and h_3, b_3 and h_4, b_4 and h_3, or b_4 and h_4 are simultaneously different from zero, and $m_M = m_G$. Inspection of the above equations shows that all non-relativistic amplitudes listed here can be written in terms of a single integral function of the integer number a, namely

$$I(a) = \int_0^1 \mathrm{d}x \int_0^{1-x} \mathrm{d}y \frac{x+y+a}{\Delta}. \qquad (C.6)$$

References

[1] R. Catena, T. Emken, N.A. Spaldin and W. Tarantino, *Atomic responses to general dark matter-electron interactions*, *Phys. Rev. Res.* **2** (2020) 033195 [arXiv:1912.08204] [INSPIRE].

[2] R. Catena et al., *Crystal responses to general dark matter-electron interactions*, *Phys. Rev. Res.* **3** (2021) 033149 [arXiv:2105.02233] [INSPIRE].

[3] Astroparticle Physics European Consortium (APPEC), http://www.appec.org/roadmap.

[4] A. Drukier and L. Stodolsky, *Principles and Applications of a Neutral Current Detector for Neutrino Physics and Astronomy*, *Phys. Rev. D* **30** (1984) 2295 [INSPIRE].

[5] M.W. Goodman and E. Witten, *Detectability of Certain Dark Matter Candidates*, *Phys. Rev. D* **31** (1985) 3059 [INSPIRE].

[6] T. Marrodán Undagoitia and L. Rauch, *Dark matter direct-detection experiments*, *J. Phys. G* **43** (2016) 013001 [arXiv:1509.08767] [INSPIRE].

[7] G. Arcadi et al., *The waning of the WIMP? A review of models, searches, and constraints*, *Eur. Phys. J. C* **78** (2018) 203 [arXiv:1703.07364] [INSPIRE].

[8] L. Roszkowski, E.M. Sessolo and S. Trojanowski, *WIMP dark matter candidates and searches — current status and future prospects*, *Rept. Prog. Phys.* **81** (2018) 066201 [arXiv:1707.06277] [INSPIRE].

[9] A. Mitridate, T. Trickle, Z. Zhang and K.M. Zurek, *Snowmass White Paper: Light Dark Matter Direct Detection at the Interface With Condensed Matter Physics*, in the proceedings of the *2022 Snowmass Summer Study*, (2022) [arXiv:2203.07492] [INSPIRE].

[10] M. Battaglieri et al., *US Cosmic Visions: New Ideas in Dark Matter 2017: Community Report*, in the proceedings of the *U.S. Cosmic Visions: New Ideas in Dark Matter*, (2017) [arXiv:1707.04591] [INSPIRE].

[11] R. Essig, J. Mardon and T. Volansky, *Direct Detection of Sub-GeV Dark Matter*, *Phys. Rev. D* **85** (2012) 076007 [arXiv:1108.5383] [INSPIRE].

[12] Y. Kahn and T. Lin, *Searches for light dark matter using condensed matter systems*, *Rept. Prog. Phys.* **85** (2022) 066901 [arXiv:2108.03239] [INSPIRE].

[13] R. Essig, T. Volansky and T.-T. Yu, *New Constraints and Prospects for sub-GeV Dark Matter Scattering off Electrons in Xenon*, *Phys. Rev. D* **96** (2017) 043017 [arXiv:1703.00910] [INSPIRE].

[14] DARKSIDE collaboration, *Constraints on Sub-GeV Dark-Matter-Electron Scattering from the DarkSide-50 Experiment*, *Phys. Rev. Lett.* **121** (2018) 111303 [arXiv:1802.06998] [INSPIRE].

[15] XENON collaboration, *Light Dark Matter Search with Ionization Signals in XENON1T*, *Phys. Rev. Lett.* **123** (2019) 251801 [arXiv:1907.11485] [INSPIRE].

[16] XENON collaboration, *Excess electronic recoil events in XENON1T*, *Phys. Rev. D* **102** (2020) 072004 [arXiv:2006.09721] [INSPIRE].

[17] P.W. Graham, D.E. Kaplan, S. Rajendran and M.T. Walters, *Semiconductor Probes of Light Dark Matter*, *Phys. Dark Univ.* **1** (2012) 32 [arXiv:1203.2531] [INSPIRE].

[18] R. Essig et al., *Direct Detection of sub-GeV Dark Matter with Semiconductor Targets*, *JHEP* **05** (2016) 046 [arXiv:1509.01598] [INSPIRE].

[19] S. Derenzo et al., *Direct Detection of sub-GeV Dark Matter with Scintillating Targets*, *Phys. Rev. D* **96** (2017) 016026 [arXiv:1607.01009] [INSPIRE].

[20] SUPERCDMS collaboration, *First Dark Matter Constraints from a SuperCDMS Single-Charge Sensitive Detector*, *Phys. Rev. Lett.* **121** (2018) 051301 [*Erratum ibid.* **122** (2019) 069901] [arXiv:1804.10697] [INSPIRE].

[21] N.A. Kurinsky, T.C. Yu, Y. Hochberg and B. Cabrera, *Diamond Detectors for Direct Detection of Sub-GeV Dark Matter*, *Phys. Rev. D* **99** (2019) 123005 [arXiv:1901.07569] [INSPIRE].

[22] DAMIC collaboration, *Constraints on Light Dark Matter Particles Interacting with Electrons from DAMIC at SNOLAB*, *Phys. Rev. Lett.* **123** (2019) 181802 [arXiv:1907.12628] [INSPIRE].

[23] EDELWEISS collaboration, *First germanium-based constraints on sub-MeV Dark Matter with the EDELWEISS experiment*, *Phys. Rev. Lett.* **125** (2020) 141301 [arXiv:2003.01046] [INSPIRE].

[24] SENSEI collaboration, *SENSEI: Direct-Detection Results on sub-GeV Dark Matter from a New Skipper-CCD*, *Phys. Rev. Lett.* **125** (2020) 171802 [arXiv:2004.11378] [INSPIRE].

[25] S.M. Griffin et al., *Silicon carbide detectors for sub-GeV dark matter*, *Phys. Rev. D* **103** (2021) 075002 [arXiv:2008.08560] [INSPIRE].

[26] S.M. Griffin et al., *Extended calculation of dark matter-electron scattering in crystal targets*, *Phys. Rev. D* **104** (2021) 095015 [arXiv:2105.05253] [INSPIRE].

[27] S. Knapen, J. Kozaczuk and T. Lin, *Dark matter-electron scattering in dielectrics*, *Phys. Rev. D* **104** (2021) 015031 [arXiv:2101.08275] [INSPIRE].

[28] Y. Hochberg et al., *Determining Dark-Matter-Electron Scattering Rates from the Dielectric Function*, *Phys. Rev. Lett.* **127** (2021) 151802 [arXiv:2101.08263] [INSPIRE].

[29] R. Lasenby and A. Prabhu, *Dark matter-electron scattering in materials: Sum rules and heterostructures*, *Phys. Rev. D* **105** (2022) 095009 [arXiv:2110.01587] [INSPIRE].

[30] H.-Y. Chen et al., *Dark matter direct detection in materials with spin-orbit coupling*, *Phys. Rev. D* **106** (2022) 015024 [arXiv:2202.11716] [INSPIRE].

[31] Y. Hochberg, Y. Zhao and K.M. Zurek, *Superconducting Detectors for Superlight Dark Matter*, *Phys. Rev. Lett.* **116** (2016) 011301 [arXiv:1504.07237] [INSPIRE].

[32] Y. Hochberg et al., *New constraints on dark matter from superconducting nanowires*, *Phys. Rev. D* **106** (2022) 112005 [arXiv:2110.01586] [INSPIRE].

[33] Y. Hochberg et al., *Detection of sub-MeV Dark Matter with Three-Dimensional Dirac Materials*, *Phys. Rev. D* **97** (2018) 015004 [arXiv:1708.08929] [INSPIRE].

[34] R.M. Geilhufe, F. Kahlhoefer and M.W. Winkler, *Dirac Materials for Sub-MeV Dark Matter Detection: New Targets and Improved Formalism*, *Phys. Rev. D* **101** (2020) 055005 [arXiv:1910.02091] [INSPIRE].

[35] A. Coskuner, A. Mitridate, A. Olivares and K.M. Zurek, *Directional Dark Matter Detection in Anisotropic Dirac Materials*, *Phys. Rev. D* **103** (2021) 016006 [arXiv:1909.09170] [INSPIRE].

[36] Y. Hochberg et al., *Directional detection of dark matter with two-dimensional targets*, *Phys. Lett. B* **772** (2017) 239 [arXiv:1606.08849] [INSPIRE].

[37] G. Cavoto et al., *Carbon nanotubes as anisotropic target for dark matter*, *J. Phys. Conf. Ser.* **1468** (2020) 012232 [arXiv:1911.01122] [INSPIRE].

[38] S. Knapen, T. Lin, M. Pyle and K.M. Zurek, *Detection of Light Dark Matter With Optical Phonons in Polar Materials*, *Phys. Lett. B* **785** (2018) 386 [arXiv:1712.06598] [INSPIRE].

[39] T. Trickle et al., *Multi-Channel Direct Detection of Light Dark Matter: Theoretical Framework*, *JHEP* **03** (2020) 036 [arXiv:1910.08092] [INSPIRE].

[40] T. Trickle, Z. Zhang and K.M. Zurek, *Detecting Light Dark Matter with Magnons*, *Phys. Rev. Lett.* **124** (2020) 201801 [arXiv:1905.13744] [INSPIRE].

[41] P. Fayet, *Effects of the Spin 1 Partner of the Goldstino (Gravitino) on Neutral Current Phenomenology*, *Phys. Lett. B* **95** (1980) 285 [INSPIRE].

[42] B. Holdom, *Two U(1)'s and Epsilon Charge Shifts*, *Phys. Lett. B* **166** (1986) 196 [INSPIRE].

[43] C. Boehm and P. Fayet, *Scalar dark matter candidates*, *Nucl. Phys. B* **683** (2004) 219 [`hep-ph/0305261`] [ɪɴSPIRE].

[44] P. Fayet, *Light spin 1/2 or spin 0 dark matter particles*, *Phys. Rev. D* **70** (2004) 023514 [`hep-ph/0403226`] [ɪɴSPIRE].

[45] XENON collaboration, *Emission of single and few electrons in XENON1T and limits on light dark matter*, *Phys. Rev. D* **106** (2022) 022001 [`arXiv:2112.12116`] [ɪɴSPIRE].

[46] XENON10 collaboration, *A search for light dark matter in XENON10 data*, *Phys. Rev. Lett.* **107** (2011) 051301 [*Erratum ibid.* **110** (2013) 249901] [`arXiv:1104.3088`] [ɪɴSPIRE].

[47] R. Catena, J. Conrad and M.B. Krauss, *Compatibility of a dark matter discovery at XENONnT or LZ with the WIMP thermal production mechanism*, *Phys. Rev. D* **97** (2018) 103002 [`arXiv:1712.07969`] [ɪɴSPIRE].

[48] B.A. Dobrescu and I. Mocioiu, *Spin-dependent macroscopic forces from new particle exchange*, *JHEP* **11** (2006) 005 [`hep-ph/0605342`] [ɪɴSPIRE].

[49] J.J. Fan, M. Reece and L.-T. Wang, *Non-relativistic effective theory of dark matter direct detection*, *JCAP* **11** (2010) 042 [`arXiv:1008.1591`] [ɪɴSPIRE].

[50] A.L. Fitzpatrick et al., *The Effective Field Theory of Dark Matter Direct Detection*, *JCAP* **02** (2013) 004 [`arXiv:1203.3542`] [ɪɴSPIRE].

[51] R. Catena and P. Ullio, *A novel determination of the local dark matter density*, *JCAP* **08** (2010) 004 [`arXiv:0907.0018`] [ɪɴSPIRE].

[52] D. Baxter et al., *Recommended conventions for reporting results from direct dark matter searches*, *Eur. Phys. J. C* **81** (2021) 907 [`arXiv:2105.00599`] [ɪɴSPIRE].

[53] T. Emken, *Dark Atomic Response Tabulator (DarkART) [Code, v0.1.0]*, https://github.com/temken/darkart (2021) [`DOI:10.5281/zenodo.6046225`].

[54] E. Urdshals and M. Matas, *QEdark-EFT*, https://zenodo.org/record/4739187 [`DOI:10.5281/ZENODO.4739187`].